MIXED MODE FATIGUE CRACK GROWTH PATH AND LIFE PREDICTION UNDER VARIABLE AMPLITUDE LOADING THROUGH EXTENDED FINITE ELEMENT METHOD

A THESIS SUBMITTED TO
THE GRADUATE SCHOOL OF NATURAL AND APPLIED SCIENCES
OF
MIDDLE EAST TECHNICAL UNIVERSITY

BY

HAYDAR DİRİK

IN PARTIAL FULFILLMENT OF THE REQUIREMENTS
FOR
THE DEGREE OF MASTER OF SCIENCE
IN
AEROSPACE ENGINEERING

JUNE 2017

Approval of the thesis:

MIXED MODE FATIGUE CRACK GROWTH PATH AND LIFE PREDICTION UNDER VARIABLE AMPLITUDE LOADING THROUGH EXTENDED FINITE ELEMENT METHOD

submitted by **HAYDAR DİRİK** in partial fulfillment of the requirements for the degree of **Master of Science in Aerospace Engineering Department, Middle East Technical University** by,

Prof. Dr. Gülbin Dural Ünver
Dean, Graduate School of **Natural and Applied Sciences** _____

Prof. Dr. Ozan Tekinalp
Head of Department, **Aerospace Engineering** _____

Assist. Prof. Dr. Tuncay Yalçınkaya
Supervisor, **Aerospace Engineering Dept., METU** _____

Examining Committee Members:

Prof. Dr. Altan Kayran
Aerospace Engineering Dept., METU _____

Assist. Prof. Dr. Tuncay Yalçınkaya
Aerospace Engineering Dept., METU _____

Assoc. Prof. Dr. Demirkan Çöker
Aerospace Engineering Dept., METU _____

Assoc. Prof. Dr. Ercan Gürses
Aerospace Engineering Dept., METU _____

Assoc. Prof. Dr. Cihan Tekoğlu
Mechanical Engineering Dept., TOBB ETU _____

Date: **22.06.2017**

I hereby declare that all information in this document has been obtained and presented in accordance with academic rules and ethical conduct. I also declare that, as required by these rules and conduct, I have fully cited and referenced all material and results that are not original to this work.

Name, Last Name: HAYDAR DİRİK

Signature :

ABSTRACT

MIXED MODE FATIGUE CRACK GROWTH PATH AND LIFE PREDICTION UNDER VARIABLE AMPLITUDE LOADING THROUGH EXTENDED FINITE ELEMENT METHOD

Dirik, Haydar

M.S., Department of Aerospace Engineering

Supervisor : Assist. Prof. Dr. Tuncay Yalçınkaya

June 2017, 79 pages

The main purpose of this study is to predict the crack growth path trajectories and fatigue crack growth (FCG) life under variable amplitude loading (VAL) by using Extended Finite Element Method (XFEM). For this purpose a computational algorithm is developed in Fortran which interacts with a commercial finite element software (Abaqus) and automatically propagates cracks which is initially modelled as stationary crack. Nasgro FCG equation is used for FCG life calculation which has a great accuracy among the FCG equations available in literature. Retardation effect due to VAL is taken into account by using appropriate retardation models according to nature of loading to show the capability of developed algorithm in covering the retardation phenomenon caused by overloads (OL) and underloads (UL). Developed algorithm is validated with several crack propagation tests available in literature in terms of crack growth path trajectories and FCG life under mode I and mixed mode loading conditions on different materials. Simulated and experimental results are in good harmony.

Keywords: Variable amplitude loading, Fatigue crack growth path, Fatigue life, XFEM

ÖZ

KARMA MODLU YORULMA ÇATLAĞININ GENİŞLETİLMİŞ SONLU ELEMANLAR METODU İLE DEĞİŞKEN GENLİKLİ YÜKLEME ALTINDA YÖRÜNGE VE ÖMÜR TAHMİNİ

Dirik, Haydar
Yüksek Lisans, Havacılık ve Uzay Mühendisliği Bölümü
Tez Yöneticisi : Yrd. Doç. Dr. Tuncay Yalçınkaya

Haziran 2017 , 79 sayfa

Bu çalışmanın temel amacı genişletilmiş sonlu elemanlar metodunu kullanarak değişken genlikli yükleme altında çatlak ilerleme yönünün ve ömrününün tahmin edilmesidir. Bu amaçla Fortran'da Abaqus ile etkileşime giren ve başlangıçta durağan çatlak olarak modellenen çatlakları otomatik olarak ilerleten bir hesaplama algoritması geliştirilmiştir. Çatlak ilerleme hesabı için literatürdeki denklemler arasında büyük bir doğruluk oranı olan Nasgro denklemi kullanılmıştır. Geliştirilen algoritmanın üst yükleme ve alt yüklemeden kaynaklı çatlak ilerleme gecikmesini hesaplayabilme kapasitesini göstermek için kullanılan yüklemenin doğasına uygun olan ilerleme gecikmesi modelleri kullanılarak ilerleme gecikmesi hesaba katılmıştır. Geliştirilen algoritma literatürde varolan catlak ilerleme testleri kullanılarak yorulma çatlağı ilerleme yönü ve ömrü açısından, birinci mod ve kompleks yükleme modlarında farklı malzemeler üzerinde doğrulanmıştır. Hesaplanan sonuçlar ile test sonuçları iyi bir uyum içerisindedir.

Anahtar Kelimeler: Değişken genlikli yükleme, Yorulma çatlağı ilerleme yörüngesi, Yorulma ömrü, Genişletilmiş sonlu elemanlar metodu

To my family and people who are reading this page

ACKNOWLEDGMENTS

I would like to express my gratitude to my supervisor Dr. Tuncay Yalçınkaya for his help, guidance and comments during this study.

I would also like to thank to my examining committee members Dr. Altan Kayran, Dr. Demirkan Çöker, Dr. Cihan Tekoğlu and Dr. Ercan Gürses for attending my thesis defence with their valuable comments and suggestions.

I would like to thank TAI for encouraging me to do a graduate study and for showing me the convenience of participating in courses during my graduate study.

I would especially like to thank to my leader at TAI, Eyüp Evren Taşkınoğlu, for his suggestions and technical supports during this study.

I would like to thank to my colleagues Fatih Özbakış, Berkay Özkan and Yezdan Medet Korkmaz for their supports and technical discussions throughout this study.

I am thankful to my friends İmam Hüseyin Taş and Senem Aktaş for their moral support during writing period of my thesis.

I express my appreciation to my brothers who supported and encouraged me during this study.

TABLE OF CONTENTS

LIST OF TABLES

TABLES

LIST OF FIGURES

FIGURES

LIST OF ABBREVIATIONS

F&DT	Fatigue and Damage Tolerance
FE	Finite Element
FEM	Finite Element Method
XFEM	Extended Finite Element Method
LFEM	Linear Elastic Fracture Mechanics
FCG	Fatigue Crack Growth
OL	Overload
UL	Underload
VAL	Variable Amplitude Loading
CAL	Constant Amplitude Loading
CT	Compact Tension
SENT	Single Edge Notched Tension
PMMA	Polymethyl Methacrylate
MTS	Maximum Tangential Stress
MERR	Maximum Energy Release Rate

LIST OF SYMBOLS

N	Number of Cycle
P_{min}	Minimum Applied Load
P_{max}	Maximum Applied Load
σ_{min}	Minimum Stress
σ_{max}	Maximum Stress
σ_{ol}	Overload Stress
σ_{ul}	Underload Stress
σ_y	Yield Stress
a	Crack Length
a_{ol}	Crack Length at Overload
a_i	Crack Length at i^{th} Cycle
R	Load Ratio
K_I	Mode I Stress Intensity factor
K_{II}	Mode II Stress Intensity factor
K_{III}	Mode III Stress Intensity factor
K_{min}	Minimum Stress Intensity Factor
K_{max}	Maximum Stress Intensity Factor
ΔK	Stress Intensity Factor Range
ΔK_{eq}	Equivalent Stress Intensity Factor Range
ΔK_{th}	Threshold Stress Intensity Factor Range
K_c	Critical Stress Intensity Factor
ΔK_0	Threshold Stress Intensity Factor Range at R=0
da/dN	Crack Growth Rate
r_{pol}	Overload Plastic Zone Size
r_{pi}	Instant Plastic Zone Size
$N_i(x)$	Shape Function for Node i
u_i	Displacement Vector for Node i
S^{ol}	Shut off Ratio

C_{th}	Curve Control Coefficient in Nasgro Equation
A_k, B_k	Fitting Parameter in Nasgro Equation
S_{max}/σ_o, α	Newman's Constant
μ	Wheeler Retardation Exponent
γ	Modified Wheeler Retardation Exponent
ϕ	Willenborg Modificaion Factor

CHAPTER 1

INTRODUCTION

Fatigue and damage tolerance (F&DT) analysis of structural components exposed to fatigue loading is a crucial issue in various industrial areas for damage tolerant designs especially in aerospace industry due to certification rules. Aerospace structures have to be replaced when the probability of failure reaches a critical level even if, it has a sufficient remaining life. Certification requirements necessitate that the damage tolerance capability of the structure have to be demonstrated with simulations and tests. To avoid unexpected results and over-conservatism, realistic fatigue crack growth (FCG) path and life prediction of components have primary importances from an economical and safety point of view. Thus, a reliable computational algorithm is needed for crack growth analysis that estimates crack propagation path and life in cyclically loaded structural components in order to prevent unexpected failure of structure in service condition. Such an algorithm reduces the high expenses of real testing facilities and replacement costs of components by estimating realistic results.

Cracks that have formed in structural components due to cyclic loadings may move straight or changes their directions depending on the loading mode. For the analysis of planar cracks under uniaxial loading a number of commercial tools have been developed that solve the FCG problem of a predefined crack under either constant or variable amplitude mode I loading condition e.g., AFGROW [1] and NASGRO [2] which use handbook solutions for stress intensity factor (SIF) and appropriate FCG rate equations available in the literature. However, industrial structures are mostly under the action of mixed mode loading condition which forms non planar crack path trajectories. The commercial tools cited above are not applicable for the case

of mixed mode loading conditions. For this reason, there is an industrial need for the tools that simulate realistic crack path and life under mixed mode loading. In the case of mixed mode loading better estimation of the cyclic life requires adopting a cycle-by-cycle summation approach based on equivalent SIF that could cover the formation of arbitrary crack shape as well as the effects of load interactions (retardations or accelerations).

An effective way for curvilinear FCG simulation is to use numerical methods such as finite element method (FEM). The conventional FEM has been used in many studies (see e.g. [3, 4, 5]) for FCG simulation with acceptable accuracy for modelling of stationary and propagating cracks. However, FEM requires considerable effort for capturing discontinuity created by cracks and some troublesome re-meshing burden in each step of crack growth analysis.

Belytschko and Black [6] developed a new Finite Element formulation called Extended Finite Element Method (XFEM) which overcomes difficulties faced during FEM simulations of crack initiation and propagation. In this method, there is no need to re-mesh during the crack propagation, which reduces the computational time and error associated with geometry mapping and mesh updating. XFEM has been validated in several works (see e.g. [9, 10, 11, 12, 13]) and it has the capability of accurately model the discontinuities such as cracks. Implementation of XFEM in Abaqus/Standard has the capability of modelling stationary cracks accurately. It also has the capability of modelling growing cracks. XFEM exercise in Abaqus uses the traction-separation cohesive behavior approach by default, instead of using fracture mechanics as stated in [14] for propagating cracks. However, the existing design certification principles for damage tolerance assessments are based on theory of Linear Elastic Fracture Mechanics (LEFM) in most industries particularly in aerospace industry. To meet the requirements of certification rules for damage tolerance assessments, a LEFM based approach should be applied. Standard implementation of XFEM in Abaqus can not deal with FCG simulations but it can effectively predict the SIF of a stationary crack tip which is the basic parameters for LEFM based damage tolerance assessments. Based on advantageous stationary crack modelling capabilities of XFEM, cost effective and practical computational algorithm in the application

of the FCG prediction under mixed mode practical service loading conditions is possible by algorithms which use externally defined analytical methods.

Industrial structures are mostly under the action of variable amplitude loading (VAL) through their service life. Although, there are many studies (see e.g. [15, 16, 17]) in the literature that analyse crack propagation under constant amplitude loading (CAL), the studies that accounts for load history effects caused by VAL are very limited. Moreover, in most of the numerical studies, cracks are propagated in manual steps, that is time consuming and has increasing risk of errors. In this respect, the need for practical and reliable computational tools in the application of the FCG path and life prediction under mixed mode loading conditions by taking into account the effect of the load history is obvious. Therefore, this area needs further investigations.

In order to eliminate the deficiencies mentioned above, the objective of this thesis is to develop a computational tool to predict the FCG path and rate by using XFEM along with available crack growth rate and path prediction methods. To achieve this purpose, a tool is developed in Fortran which automatically propagates stationary modelled cracks step by step. This algorithm interacts with Abaqus environment and determine the FCG path and life by using embedded equations into the algorithm under user defined load spectra. The Nasgro equation that is commonly used in aerospace practices is used in the algorithm for life calculations through the simulations. Stationary initial cracks propagated by using $K_{II} = 0$ criterion proposed by Cotterell and Rice [18]. The load history effect is also taken into account by embedding the modified form of Wheeler [19] and Willenborg [20] retardation models to the developed algorithm.

The preliminary results of the method for planar cracks under uni-axial loading conditions have recently been presented in 21^{th} European Conference on Fracture [21] and National Aviation and Space Conference (6^{th} UHUK)[22] by Dirik and Yalçınkaya. Developed algorithm is also verified for the case of curvilinear crack propagation in terms of crack path trajectories and FCG life in several specimens which has experimental results in open literature. The results are in good harmony.

1.1 Outline of Thesis

This thesis is presented through five chapters. An introduction is presented in chapter 1 which includes motivation objective and contribution of this study.

The theoretical background and literature review about crack growth life, crack growth path, retardation models and XFEM are given in Chapter 2 .

Main structure of the developed computational procedure is described in Chapter 3 by presenting an algorithm chart and giving the details on each step.

Several numerical case studies presented in Chapter 4 for the validation of the developed algorithm with the experimental results available in the literature in terms of FCG path and life under different loading conditions for different materials.

Finally, Chapter 5 is devoted to discussion, concluding remarks and possible future works.

CHAPTER 2

THEORETICAL BACKGROUND AND LITERATURE REVIEW

This chapter reviews theoretical background of basic terms and methods used in developed computational algorithm such as the stress intensity factor (SIF), crack path prediction models, life prediction models and retardation phenomena. Extended finite element method (XFEM) was also explained in this chapter together with some crack modelling tips in Abaqus by using XFEM. Along with this review a summary of the previous work done in the literature are presented as well with their advantages and limitations.

2.1 Stress Intensity Factor

As the radius of the curvature at crack tip approaches zero, the stress level goes to infinity which is not a realistic behaviour of the structure. In such cases, the stress concentration factor, a parameter that determines behaviour of the structure, no longer reflects real behaviour of the structure and can not be used. As an alternative way, SIF can be used appropriately to represent the stress field at the crack tip. For this reason, SIF has an important role in fatigue and damage tolerance (F&DT) assessments. At critical levels of SIF, cracks can be initiated, the initiated cracks may growth and eventually catastrophic failure of the components might occur. SIF's depend on the mode of loading and crack configurations. There are three different modes of loading used in fracture mechanics. These are mode I loading, mode II loading and mode III loading.

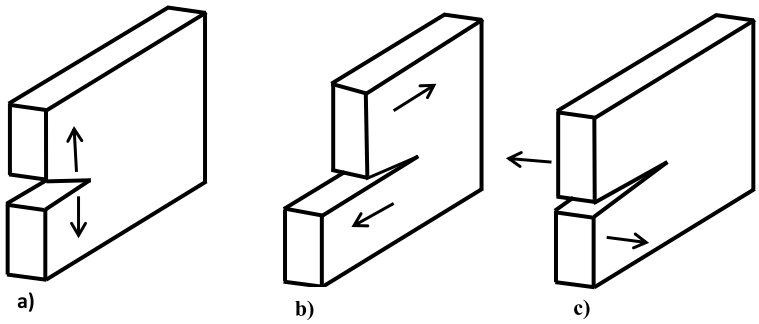

Figure 2.1: Loading modes a) Mode I b) Mode II c) Mode III.

Mode I is the crack opening mode, mode II is an in-plane shear mode and mode III is an out-of-plane shear mode as illustrated respectively in Figure 2.1. By using the stress state near the crack front presented in Figure 2.2, the SIF for three different loading mode can be calculated through equations (2.1)-(2.3) for mode I, mode II and mode III respectively. Where σ_{ij} represents the normal or shear stresses components in the specified directions. The SIF is related to the nominal stress level (σ) and the size of the crack (a). In general, the relation for SIF is represented by $K = f(a/w)\sigma\sqrt{\pi a}$ where $f(a/w)$ is a geometric correction factor which depends on structural member and crack length. The values of $f(a/w)$ for standard specimen can be found in handbooks.

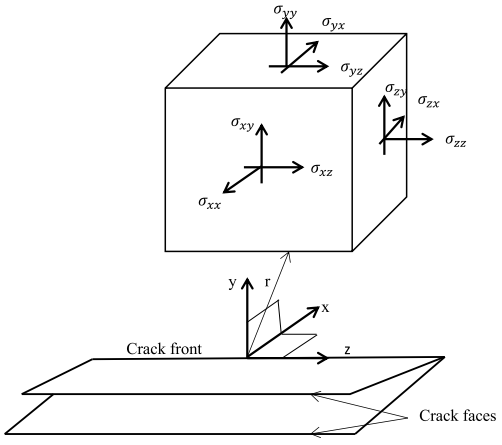

Figure 2.2: Three dimensional stress state at crack front.

Expression of SIF for different modes are given as,

$$K_I = \lim_{r \to 0} \sqrt{2\pi r}\sigma_{yy}\left(r, 0\right). \tag{2.1}$$

$$K_{II} = \lim_{r \to 0} \sqrt{2\pi r}\sigma_{yx}\left(r, 0\right). \tag{2.2}$$

$$K_{III} = \lim_{r \to 0} \sqrt{2\pi r}\sigma_{yz}\left(r, 0\right). \tag{2.3}$$

2.2 Mixed Mode Stress Intensity Factor

In the case of mixed mode loading better estimation of the FCG life in cyclic loading needs an equivalent SIF range that could cover the non planar crack formation. Several studies on the mixed mode loading have been conducted in the literature to determine a reasonable and applicable equivalent SIF range from ΔK_I and ΔK_{II}. The most important ones of these studies can be mentioned as following.

Tanaka [23] proposed one of the most striking examples and made a significant contribution for the determination of mixed mode equivalent SIF range (ΔK_{eq}) which is based on the idea that cracks can propagate if the displacement behind the crack tip reaches a critical value. Tanaka's equivalent SIF expression is given as,

$$\Delta K_{eq} = \left[\Delta K_I^4 + 8\Delta K_{II}^4\right]^{0.25}. \tag{2.4}$$

Richard [24] presented an empirical equation for the estimation of equivalent SIF range in which Mode I (K_{Ic}) and Mode II (K_{IIc}) fracture toughness are used. Richard's equation for mixed mode SIF is expressed as,

$$\Delta K_{eq} = \frac{1}{2}K_I + \frac{1}{2}\sqrt{K_I^2 + 4\left(\frac{K_{Ic}}{K_{IIc}}K_{II}\right)^2}. \tag{2.5}$$

Tong and Yan [25] suggested another effective SIF concept which is simple extension of the maximum tangential stress (MTS) criterion [26] to the case of mixed mode FCG. Tong and Yan equivalent SIF description is given as,

$$\Delta K_{eq} = \frac{1}{2}cos\left(\frac{\theta_0}{2}\right)\left[\Delta K_I(1 + cos(\theta_0)) - 3\Delta K_{II}sin(\theta_0)\right] \tag{2.6}$$

where θ_0 is the crack growth direction proposed by Erdogan and Sih [26] in MTS criterion.

Hoshide [28] and Chen [29] also suggested relations for crack growth rate using J integral for mixed mode situations. Among all these models, the mostly used one is Tanaka's model which has substantial experimental correlations, which is reliable and easy to use. Therefore, in this study, Tanaka's model is implemented to the developed algorithm because of its mentioned advantages.

2.3 Crack Growth Life

FCG life is generally predicted by using an exponential function of SIF range ΔK in LEFM. The SIF range ΔK is the basic term in determination of crack growth rate da/dN. A log-log plot of da/dN vs. ΔK is shown in Figure 2.3. In this diagram, Region I is the crack initiation interval in which crack growth rate approaches to zero. Region II is the stable crack growth interval. Paris equation accounts for this stable crack growth interval. Region III is unstable crack growth interval in which crack growth rate is very high and FCG life is very short. In this final fracture region, maximum SIF reaches the critical level (K_c), which eventually results with fracture.

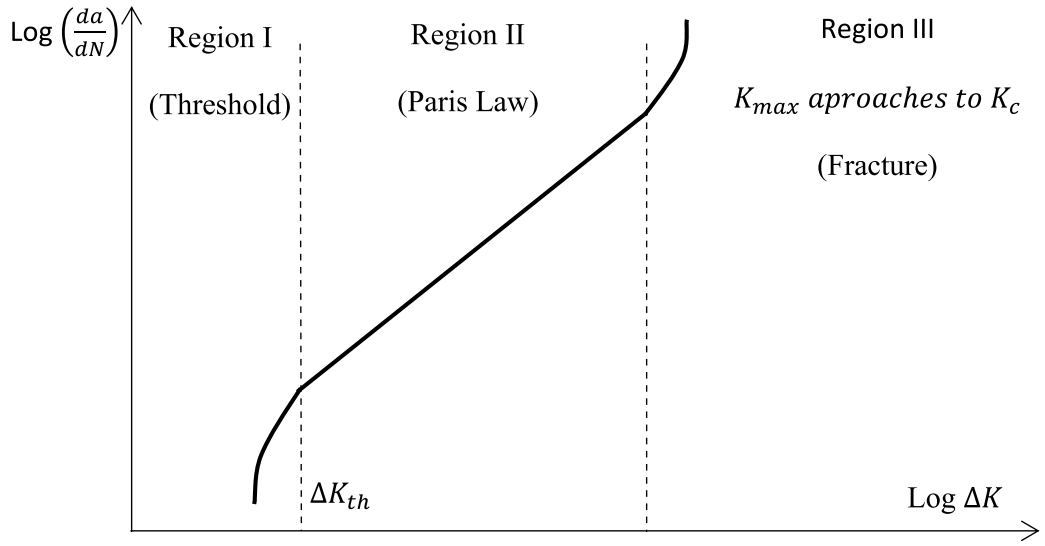

Figure 2.3: da/dN vs. ΔK diagram.

There are various studies in literature to estimate the FCG rate (da/dN) for FCG life calculations. The first pioneering work is suggested by Paris and Erdoğan [30] that introduced a SIF based tentative relation known as Paris equation,

$$\frac{da}{dN} = C\left(\Delta K\right)^n \tag{2.7}$$

where, N is the number of applied load cycles, a is the crack length, ΔK is the SIF range. C and n are empirically determined material constants. Paris equation only covers the Region II of the da/dN vs. ΔK diagram. This pioneering equation was modified by several researcher over time.

Walker [31] modified the Paris equation to account for the stress ratio $R = K_{min}/K_{max}$. Walker equation only incorporates the effect of mean stress to the Paris equation. It does not account for Region I and III of the crack growth rate curve in low and high level of SIF range and presented as,

$$\frac{da}{dN} = C\left[\frac{\Delta K}{\left(1-R\right)^{1-\gamma}}\right]^m \tag{2.8}$$

where C, m and γ are the material dependent empirical constants. Values of γ ranges from 0.3 to 1 for various metals. Lower values of parameter γ means a strong dependence of FCG rate to the mean stress.

Forman et al. [32] suggested a further modification on Paris law that incorporates the parameter of critical SIF (fracture toughness) to the equation to account for Region III of the da/dN vs. ΔK diagram as follow,

$$\frac{da}{dN} = \frac{C\left(\Delta K\right)^n}{\left(1-R\right)\left(K_c - K_{max}\right)}. \tag{2.9}$$

Hartman and Schijve [33] suggested another update on Paris law by adding a parameter of threshold SIF range to cover the Region I of da/dN vs. ΔK curve which is initiation interval,

$$\frac{da}{dN} = D\left[\frac{\left(\Delta K - \Delta K_{th}\right)}{\sqrt{1 - K_{max}/A}}\right]^\alpha \tag{2.10}$$

where D, A and α are empirical material constants and ΔK_{th} is the threshold SIF range.

Throughout the years, many contributions were done for the update of the FCG rate relations and the efforts are converged to a commonly used equation referred to as the Nasgro equation (also called Forman- Newman-de Koning equation) which is expressed in (2.11). Nasgro equation is based on the Forman [34] relation and consider plasticity-induced crack closure by using the crack opening function introduced by Newman [35].

Nasgro equation is commonly used as a state of the art practice in major industries particularly in aerospace industry in FCG assessments for CAL and VAL conditions. It covers all regions (Region I, II and III) of the da/dN vs. ΔK diagram by taking into account the R-ratio effect, the threshold value of the SIF range ΔK_{th} and the fracture toughness of the material (K_c). The expression for Nasgro equation is given as,

$$\frac{da}{dN} = C\left(\frac{1-f}{1-R}\Delta K\right)^n \frac{\left(1-\frac{\Delta K_{th}}{\Delta K}\right)^p}{\left(1-\frac{\Delta K_{max}}{\Delta K_c}\right)^q} \tag{2.11}$$

where, N is the number of load cycles, a is the crack length, ΔK is the SIF range, ΔK_{th} is the threshold SIF range, K_c is the fracture toughness of the material C, n, p and q are material constants. Here f is defined as,

$$f = \begin{cases} R, A_0 + A_1 R + A_2 R^2 + A_3 R^3, & \text{for } R \geq 0 \\ A_0 + A_1, & \text{for} -2 \leq \ R \leq 0 \end{cases}$$

where, A_0, A_1, A_2, A_3 are given as,

$$\begin{aligned} A_0 &= (0.825 - 0.34\alpha + 0.05\alpha^2)\left[cos\left(\frac{\pi}{2}\frac{S_{max}}{\sigma_0}\right)\right]^{\frac{1}{\alpha}} \\ A_1 &= 0.415 - 0.071\left[\alpha\frac{S_{max}}{\sigma_0}\right] \\ A_2 &= 1 - A_0 - A_1 - A_3 \\ A_3 &= 2A_0 + A_1 - 1 \end{aligned} \tag{2.12}$$

α and S_{max}/σ_0 appearing in the expressions for A_0 and A_1 are the Newman's canstants. α is a constant which ranges from 1 to 3. The ratio of the maximum stress S_{max} to the flow stress σ_0 is fixed to 0.3 for most of the materials. In the present work, the

values of α and $\frac{S_{max}}{\alpha_0}$ were used as proposed by Nasgro material database.

The threshold SIF range in (2.11) can be calculated as,

$$\Delta K_{th} = \Delta K_0 \sqrt{\frac{a}{a+a_0}} \left[\frac{1-f}{(1-A_0)(1-R)} \right]^{-(1+C_{th}R)} \tag{2.13}$$

where, a_0 is an intrinsic crack size which depends on the material grain size, ΔK_0 is the threshold SIF at $R = 0$ and C_{th} is the curve control coefficient for different R ratios. The effect of thickness is considered by using the critical SIF (K_c) as below

$$\frac{K_c}{K_{Ic}} = 1 + B_k e^{-(A_k t/t_0)^2} \tag{2.14}$$

where A_k and B_k are fitting parameters, t is the thickness and t_0 is the reference thickness related to plane strain condition that is calculated as follows,

$$t_0 = 2.5 \frac{{K_{Ic}}^2}{\sigma_y} \tag{2.15}$$

where σ_y is the yield stress.

There are several examples in literature where Nasgro equation captures the fatigue life of cracked components with a good accuracy (see e.g. [36], [37] and [38]). The coefficients of Nasgro equation have reported for most of the engineering materials in Nasgro software material database [2].

2.4 Crack Propagation Path

In industrial structures, the cracks usually propagate by changing its direction depending on the mode of loading conditions. Many criteria have been proposed in literature for path prediction of growing cracks. The sounding works on the crack path evaluation can be mentioned as following.

Erdoğan and Sih [26] proposed the maximum tangential stress (MTS) criterion which indicates that; a crack growth occurs when MTS reaches a critical level and crack extent in radial direction corresponding to this maximum stress direction. Its mathe-

matical formulation is represented as,

$$\theta_c = 2tan^{-1}\left[0.25\left[\frac{K_I}{K_{II}} \pm \sqrt{\left(\frac{K_I}{K_{II}}\right)^2 + 8}\right]\right] \tag{2.16}$$

where θ_c is the crack growth angle.

Palaniswamy and Knauss [40] recommend the maximum energy release rate criterion (MERR) which says crack extension occurs in the direction which maximize the energy release rate dU/dA where U is the potential of the system.

Maiti and Smith [42] proposed another approach which is known as maximum tangential principal stress (MTPS) which indicates maximum tangential stress as a principal stress and crack extension assumed to occurs in this principal direction. These criteria have in common that, when second mode SIF at the crack tip is non zero, then the crack extension follow a path which is continuously change its direction.

In this study, the criterion of local symmetry ($K_{II} = 0$ criterion) suggested by Cotterel and Rice [18] is used in crack growth simulations which is already implemented in Abaqus. Criterion of local symmetry have been shown to provide good accuracy in literature (see e.g. [43]). This criterion can be explained by considering an infinitesimally small kinged crack shown in Figure 2.4. The mode I and II SIF's, k_I^k and k_{II}^k at the tip of the putative crack can be represented in terms of SIF's K_I and K_{II} of the parent crack as presented in (2.17).

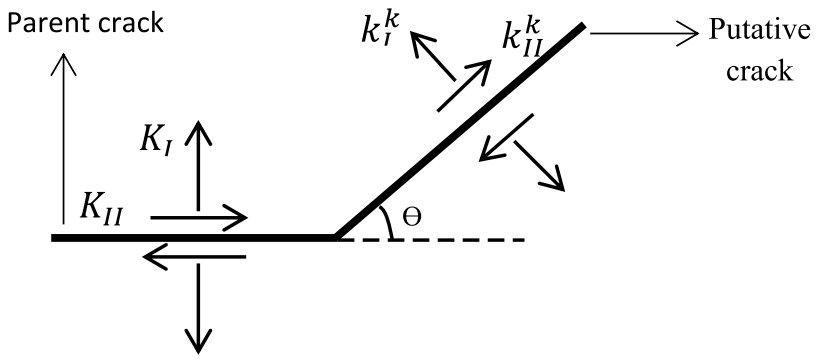

Figure 2.4: Schematic representation of kinked crack.

$$
\begin{aligned}
k_I^k &= C_{11}K_I + C_{12}K_{II} \\
k_{II}^k &= C_{21}K_I + C_{22}K_{II}
\end{aligned}
\tag{2.17}
$$

The C_{mn} appearing above depend on polar kinking angle θ as follows [40].

$$
\begin{aligned}
C_{11} &= \frac{1}{4}\left[3\cos\frac{\theta}{2} + \cos\frac{3\theta}{2}\right] \\
C_{12} &= \frac{-3}{4}\left[\sin\frac{\theta}{2} + \sin\frac{3\theta}{2}\right] \\
C_{21} &= \frac{1}{4}\left[\sin\frac{\theta}{2} + \sin\frac{3\theta}{2}\right] \\
C_{22} &= \frac{1}{4}\left[\cos\frac{\theta}{2} + 3\cos\frac{3\theta}{2}\right]
\end{aligned}
\tag{2.18}
$$

$K_{II} = 0$ criterion simply postulates that a crack will initially propagate in the direction that makes k_{II}^k equal to zero

$$
k_{II}^k = \frac{1}{4}\left[\sin\frac{\theta}{2} + \sin\frac{3\theta}{2}\right] K_I + \frac{1}{4}\left[\cos\frac{\theta}{2} + 3\cos\frac{3\theta}{2}\right] K_{II}. \tag{2.19}
$$

2.5 Retardation Phenomena

The crack growth rate under CAL condition alters if the structure is under the action of VAL condition. Significant acceleration or retardation might occur in crack growth rate due to applied OL or UL. Therefore, the loading history have to be considered in FCG life calculations for better estimations. An OL immediately applied after CAL cause to delay in crack growth rate at subsequent load cycles, while a subsequently applied OL-UL reduce the positive effect of the OL on crack growth rate. The mentioned retardation effects are presented in Figure 2.5 [41].

Many crack growth retardation models are available in literature to take into account load history effect on the FCG life. The first category of these model is based on yield zone size (see e.g. Wheeler [19] and Willenborg et. al [20]). The second category is based on an effective SIF range ΔK_{eff}. The effective SIF is the difference between

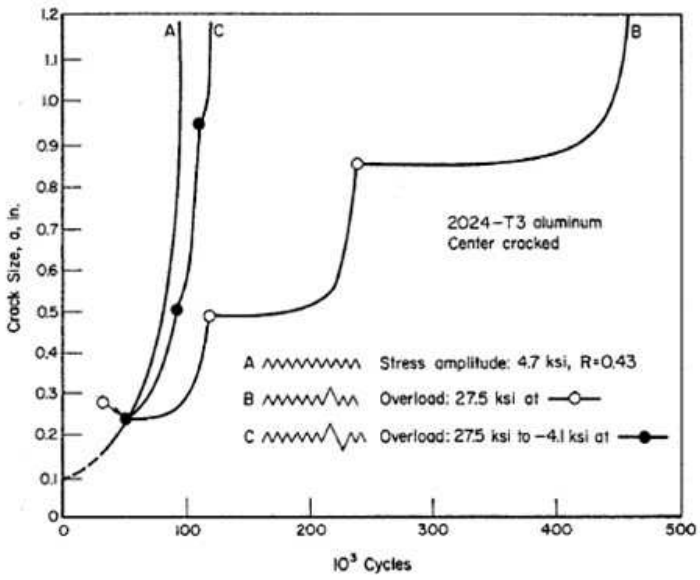

Figure 2.5: Retardation phenomena for OL and OL-UL. [41]

the applied SIF and the SIF for crack closure. These models contain many empirical constants, which make them difficult to use. In this work, only the first category is considered. Yield zone models are easy to use and the number of experimental parameters are relatively less compared to closure models. The yield zone models assume that, if the size of the plastic zone developed by the current load cycle extends the previously developed plastic zone size there will be no retardation on crack growth. Otherwise, the crack growth rate will be retarded. Figure 2.6 shows the relation between crack size and plastic zone.

Point to note is that, the specimen thickness has important influences on crack growth rate behaviour of the specimen. Therefore, the size of the plastic zone at crack tip is larger in thin specimen than for thick specimen. Such cases can be considered theoretically by assuming plane stress or plane strain condition for thin or thick specimen, respectively. In the examined crack growth cases in this study for complex stress field in the vicinity of the crack tip a plane stress assumption is made according to their thickness. State of plain strain domination needs a specimen thickness that is sufficiently large.

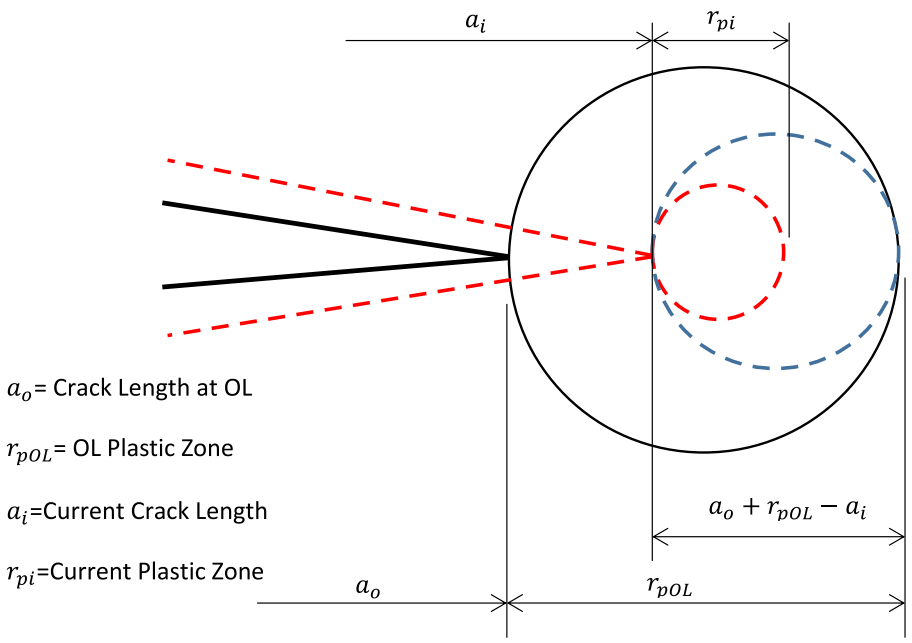

Figure 2.6: Crack tip yield zone.

The size of instant cyclic plastic zone (r_{pi}) and and monotonic OL plastic zone (r_{pol}) can be calculated by adopting following equations,

$$r_{pi} = \frac{1}{\pi}\left(\frac{\Delta K_{eq}}{2\sigma_y}\right)^2 \tag{2.20}$$

$$r_{pol} = \frac{1}{\pi}\left(\frac{K_{ol}}{\sigma_y}\right)^2 \tag{2.21}$$

In here, ΔK_{eq} is the equivalent SIF range and K_{ol} is the SIF caused by OL and σ_y is the yield strength of the material. The first yield zone model used in this study is a modified form of Wheeler model [19] and it has good agreement with experimental studies when single OL applied periodically on a CAL spectrum. In Wheeler model, delayed crack growth rate caused by tensile OL is covered by,

$$\left[\frac{da}{dN}\right]_{ret,i} = C\left[\frac{da}{dN}\right]_i. \tag{2.22}$$

The value of retardation constant C is determined as follow, where μ is an experimentally adjustable retardation parameter.

$$C = \begin{cases} \left[\dfrac{r_{pi}}{r_{pol} + a_{ol} + a_i}\right]^{\mu}, & \text{for } a_i + r_{pi} \leq a_{ol} + r_{pol} \\ 1, & \text{for } a_i + r_{pi} \geq a_{ol} + r_{pol} \end{cases}$$

$\left[\frac{da}{dN}\right]_{ret,i}$ and $\left[\frac{da}{dN}\right]_i$ are the retarded and corresponding non-retarded crack growth rates respectively. a_{ol} and a_i are the crack sizes at the instances; just after the application of the OL and at the subsequent i^{th} cycle respectively. Wheleer model has lack of the capability to cover the crack arrest since the value of calculated $\left[\frac{da}{dN}\right]_{ret,i}$ is always positive.

Meggiolaro et. al [44] suggested a modification on the original Wheeler model. By this modification both crack retardation and arrest can be predicted. This approach called the Modified Wheeler model and uses a parameter γ to multiply ΔK instead of multiplying $\left[\frac{da}{dN}\right]_i$ after the OL. In this model retardation is covered by using a retarded SIF range,

$$\Delta K_{ret}(a_i) = C\Delta K(a_i). \tag{2.23}$$

The value of retardation constant C is determined as follows,

$$C = \begin{cases} \left[\dfrac{r_{pi}}{r_{pol} + a_{ol} + a_i}\right]^{\gamma}, & \text{for } a_i + r_{pi} \leq a_{ol} + r_{pol} \\ 1, & \text{for} a_i + r_{pi} \geq a_{ol} + r_{pol} \end{cases}$$

where γ is an experimentally adjustable retardation parameter and generally different from the original Wheeler model retardation exponent μ. $\Delta K_{ret}(a_i)$ and $\Delta K(a_i)$ are the values of the SIF ranges that would be used at a_i with and without retardation due to OL respectively. This simple modification can be used with any of the crack propagation equations that takes into account the effect threshold SIF range ΔK_{th} in determination of both retardation and arrest of fatigue cracks after an OL. The arrest occurs if $\Delta K_{ret}(a_i) > \Delta K_{th}$.

The second yield zone model used in this study is a modified form of Willenborg model [20] which consider the effects crack growth retardation by using an effective SIF concept supplied as $K_i^{eff} = K_i - K_R$ in which K_i is the typical SIF for the i^{th} cycle and K_R is the residual SIF,

$$K_R = K_R^W = K_{max}^{ol}\sqrt{1 - \frac{a_i - a_{ol}}{r_{p,ol}}} - K_{max,i} \tag{2.24}$$

where a_i instant crack size, a_{ol} crack size at the application of OL, $r_{p,ol}$ the yield zone produced by the OL, K_{max}^{ol} maximum SIF of the OL and $K_{max,i}$ maximum SIF for

the current cycle. Willenborg et al. [20] model can not deal with effect of UL either.

Gallagher and Hughes [46] generalized the Willenborg model by modifying the residual SIF used in this model with an experimental material dependent constant. This generalized model can only cope with OL effect. They proposed that $K_R = \Phi K_R^W$ where Φ is given as,

$$\Phi = \frac{1 - \dfrac{K_{max,th}}{K_{max,i}}}{S^{ol} - 1}. \tag{2.25}$$

In which $K_{max,th}$ is the threshold SIF level related to the zero FCG rates and S^{ol} is shut-off ratio required to cause crack arrest for the given material. In this model retardation effect is sensed by the change in the effective stress ratio.

$$R_{eff} = \frac{K_{min,i}^{eff}}{K_{max,i}^{eff}} = \frac{K_{min,i} - K_R}{K_{max,i} - K_R} \tag{2.26}$$

Thus, for the i^{th} load cycle, the crack growth increment Δa_i is given by,

$$\Delta a_i = \frac{da}{dN} = f(\Delta K, R_{eff}). \tag{2.27}$$

Brussat et. al [47]) suggest a further modification on Generalized Willenborg model to consider for the effect of UL also. In this modification a factor Φ is used which is given as follows,

$$C = \begin{cases} \Phi = 2.523\Phi_0/(1 + 3.5(0.25 - R_U))^{0.6}, & \text{for } R_U < 0.25 \\ \Phi = 1, & \text{for } R_U \geq 0.25 \end{cases}$$

where R_U is the ratio of current UL stress (σ_{ul}) to OL stress (σ_{ol}) and Φ_0 is a material and spectrum dependent parameter which typically ranges from 0.2 to 0.8.

2.6 Extended Finite Element Method (XFEM)

A new finite element technique called XFEM has been developed by Belytschko and Black [6] to overcome the difficulties encountered in traditional FEM modeling of discontinuities such as craks. The mathematical background behind XFEM is the partition of unity concept presented by Melenk and Babuska [7]. Partition of unity

specified by a set of n functions f_i that fulfilling the requirement $\sum_{i=1}^{n} f_i(x) = 0$. Using the concept of local partition of unity makes it possible to enrich the FE approximation space. This enrichment in XFEM allows the discontinuities and singularities around the crack to be represented independent from FE mesh. The objective in representing discontinuities is simply to represent mesh 1 shown in Figure 2.7 by using mesh 2 plus some enrichment terms.

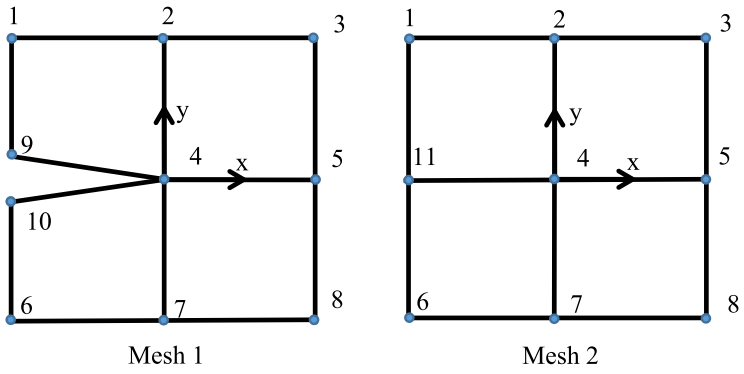

Figure 2.7: Mesh configurations.

XFEM displacement solution is given by

$$u(x,y) = \sum_{i=1}^{10} N_i(x,y)(u_i) \tag{2.28}$$

In here, $N_i(x,y)$ is the shape function for node i and u_i is the displacement vector for the same node. By taking the average value of u_9 and u_{10} as m and the distance between the two nodes as n, it is appropriate to write

$$m = (u_9 + u_{10})/2 \tag{2.29}$$

$$n = (u_9 - u_{10})/2 \tag{2.30}$$

From these equalities, u_9 and u_{10} can be written written as $m + n$ and $m - n$ respectively. Then, the expression for displacement solution can be written as,

$$u(x,y) = \sum_{i=1}^{8} N_i(x,y)(u_i) + m(N_9 + N_{10}) + n(N_9 + N_{10})H(x,y) \tag{2.31}$$

where H(x,y) is the jump function represented as

$$H(x,y) = \begin{cases} 1, & \text{for } y > 0 \\ -1, & \text{for } y < 0 \end{cases}$$

In (2.31) N_{11} can be substituted for $N_9 + N_{10}$ and u_{11} can be substituted for m. Then, the displacement expression can be rearranged as,

$$u(x,y) = \sum_{i=1}^{8}(N_i(x,y)(u_i) + N_{11}u_{11}) + (nN_{11})H(x,y)). \tag{2.32}$$

The first term of the equation corresponds to the conventional approach by the FEM, and the second term represents the jump enrichment for new node with displacement u_{11} and hence new degrees of freedom. The equation (2.32) tells us that the geometry of a crack can be represented by a mesh which does not contain any discontinuity.

To illustrate picking up the existing singularities, let all nodes be represented by the set D, the nodes around crack the tips and faces are represented by the sub set D_t and D_c respectively. Then, the approach for displacement calculation for crack modelling in XFEM has such a form given by,

$$u_{xfem} = \sum_{i\in D} N_i(x)(u_i) + \sum_{i\in D_c} N_i(x)H(x)(a_i) + \sum_{i\in D_t}\left[N_i(x)\sum_{\alpha=1}^{4} F_\alpha(x)b_i^\alpha\right] \tag{2.33}$$

where, u_{xfem} is the displacement vector, N_i is the nodal shape function, u_i is the nodal displacement vector for non-enriched nodes, $H(x)$ is the Heaviside function which is $+1$ on one side of the discontinuity and -1 on other side of the discontinuity, $a(i)$ is the nodal enriched degree of freedom vector associated with Heaviside function, b_i^c is the nodal enriched degree of freedom vector associated with crack tip enrichment. $F_\alpha(x)$ are the asymptotic crack tip functions for linear elastic isotropic materials,

$$\left\{F_\alpha\left(x\right)\right\}_{i=1}^{4} = \left(\sqrt{r}sin(\alpha/2), \sqrt{r}cos(\alpha/2), sin(\alpha/2)sin(\alpha), cos(\alpha/2)sin(\alpha)\right). \tag{2.34}$$

The main advantage of XFEM compared with the traditional FEM is that, it is not needed for FE mesh to conform the boundaries of the geometric discontinuities such as cracks. So the user gets rid of the troublesome burden of re-meshing in each step

of crack growth analysis. In this way, XFEM gives a great flexibility to the user in modelling discontinuities. The main goal in using XFEM is not determination the stresses, strains or displacements. The interest here is to the determine the SIF for available cracks. Similar to the traditional situation, the evaluation of SIF in XFEM is based on evaluation of interaction integral over the crack tip area. Crack propagation directions is determined by using the calculated SIF in appropriate crack path prediction models available in literature. There are three criteria for crack path determination implemented already into Abaqus for homogeneous, isotropic linear elastic materials, these are the maximum tangential stress (MTS) criterion, the maximum energy release rate (MERR) criterion and the $K_{II} = 0$ criterion.

XFEM has taken the attention of users in modelling stationary and propagating cracks since it was introduced in 1999. Many authors have applied XFEM to model stationary and growing cracks. Some of these attempts can be mentioned as follows.

Shi et al. [8] developed and implemented a 3D XFEM coupled with a narrow band fast marching method in the Abaqus FE package for curvilinear FCG path and life evaluation in metallic structures. Giner et al. [11] suggested an implementation of XFEM for 2D LEFM applications with multiple cracks. Sukumar and Prevost [9], presented a fortran implementation of the XFEM to a general purpose FE package for modelling 2D cracks in isotropic and bimaterial media. The 3D X-FEM together with the level set method was used to simulate curvilinear crack growth in [48] and [49].

Due to many captivating features of X-FEM, several other attempts have been made to implement XFEM to commercial FEM packages for SIF evaluation and crack path determination (see e.g.[10, 11]). XFEM has also been validated in several works (see e.g. [12, 13]) and it has the capability of accurately model the discontinuities such as cracks. Therefore, It is possible to develop efficient tools in terms of practicality and reliability in industrial applications based on the valuable contributions made in this field.

2.7 XFEM in ABAQUS

As discussed previously, stationary and propagating cracks can be modelled through XFEM crack modelling capability of Abaqus. The SIF calculation in Abaqus through XFEM is performed along the crack front for a finite number of nodes. These nodes are called as contour integral evaluation points. The number of contours to be included in the contour domain must be specified to calculate the SIF. These contours are automatically determined by Abaqus at points where the crack tip intersects the element boundaries. A schematic description of the element rings in Abaqus can be seen in Figure 2.8. The first partial contour domain consists of the elements surrounding the crack tip. The next partial contour domain contains the first domain and the next element ring directly connected to the first contour field. The contour integral calculation is theoretically independent from the size of the contour but due to the approximation with a FE solution, the SIF for the different element contour differs slightly from each other. The demonstration of effect of requested number of contours on SIF value is given in next section on a simple case study for the justification of SIF extraction method through the whole study.

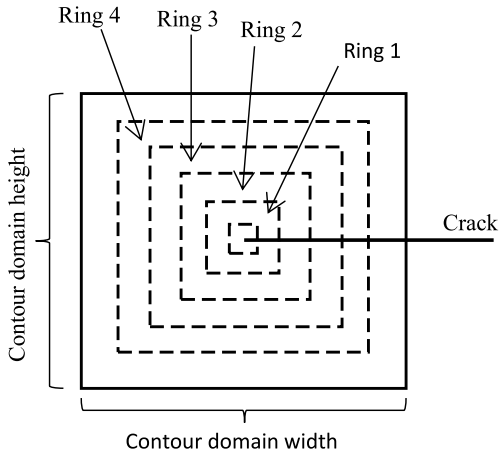

Figure 2.8: Contour domain in Abaqus.

The main difference between stationary and propagating crack modelling in XFEM is the enrichment procedure. Different enrichment functions and number of enriched nodes are considered in XFEM for stationary and propagating cracks as illustrated in

Figure 2.9. For stationary cracks, the nodes located on crack tip and crack face elements are enriched with Heaviside function and the asymptotic near-tip singularity functions. While the nodes located on the crack face elements are enriched only with the Heaviside function.

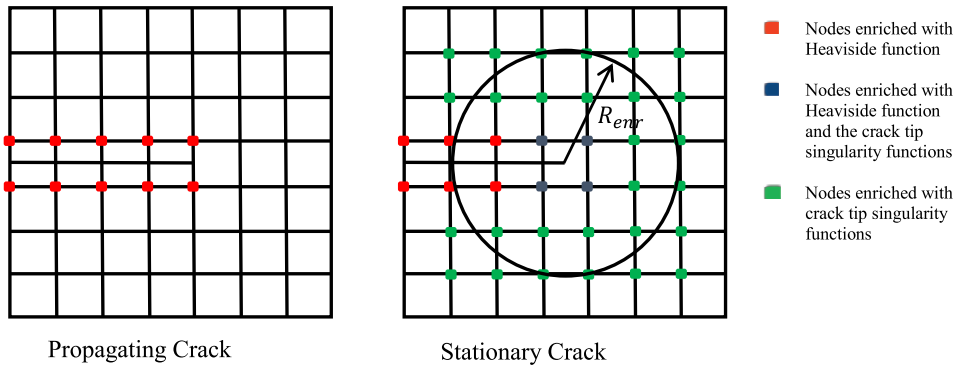

Figure 2.9: Enrichment procedure in Abaqus.

The enrichment radius shown in Figure 2.9 can be determined by the user. Higher the enriched number of nodes means higher accuracy [8] with additional computational cost. The enrichment radius is used as recommended by the analysis default in Abaqus/Standard as three times the element characteristic length through all study. Current implementation of XFEM available in Abaqus/Standard has some constraints. The most important ones can be listed as below.

- XFEM currently not available in Abaqus/Explicit. It supports only static and implicit dynamic analysis in Abaqus/Standard.
- Stationary crack analysis can only be modelled with linear elastic materials.
- Only 1^{st} order 3D solid continuum elements are supported for stationary cracks.
- Only 1^{st} order 2D and 3D solid continuum elements, and 2^{nd} order tetrahedron elements are supported for propagating cracks analysis.
- XFEM has some convergence issues in propagating crack analysis.
- XFEM has not the capability to capture crack branching.
- As declared in [14], standard implementation of XFEM has not the capability to model fatigue crack growth.

2.7.1 SIF Extraction from XFEM Solution

The SIF's are obtained by performing a J integral calculation in Abaqus as stated in [14]. The calculation of SIF from a known J integral is not straightforward for mixed-mode problems. Abaqus uses an interaction integral method to compute the SIF's directly for a crack under mixed-mode loading.

The J integral is a contour integral for 2D geometries (see figure 2.10) and can be extended to 3D geometries.

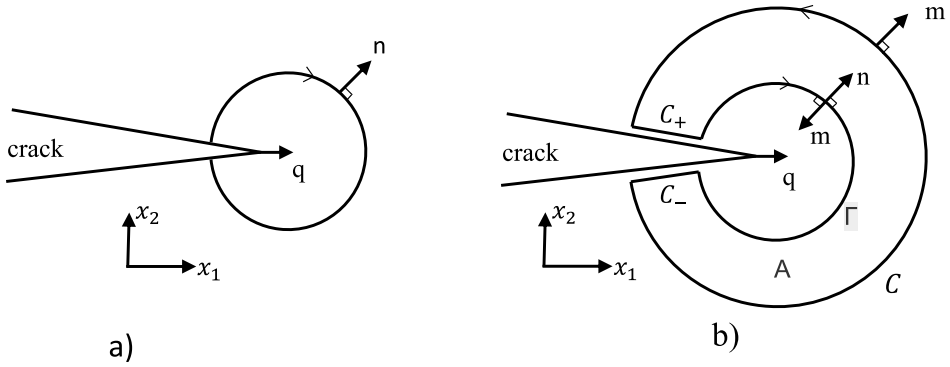

Figure 2.10: a) 2D contour integral, b) 2D closed contour integral.

For the 2D case, the J-Integral can be written as [50]

$$J = \lim_{\Gamma \to 0} = \int_{\Gamma} n \cdot H \cdot q \, d\Gamma \tag{2.35}$$

where Γ is the contour which connected to the crack faces and enclose the crack tip, n is the exterior normal of the contour, and q is the unitary vector within the virtual extension direction of the crack. The function H is defined by,

$$H = W \cdot I - \sigma \cdot \frac{\partial u}{\partial x} \tag{2.36}$$

where W is the elastic strain energy, I is the identity tensor, σ is the stress tensor and u is the displacement vector.

The 2D contour integral can be rewritten as a 2D closed contour integral as [50]

$$J = \oint_{C+C_++\Gamma+C_-} m \cdot H \cdot \bar{q} \, d\Gamma - \int_{C_++C-} t \cdot \frac{\partial u}{\partial x} \cdot \bar{q} \, d\Gamma \tag{2.37}$$

where the contours, Γ, C, C_+ and C_- are shown in Figure 2.10. The normal m has introduced as the unitary exterior normal to the contour C, respecting $m = -n$. Here also the weighting function $\bar{q}$ has been introduced as an unit vector applied in the direction of the virtual extension of the crack tip, which respects $\bar{q} = q$ in Γ and vanishes on C. In equation (2.37), t is the traction on the crack surfaces. Traction on the crack surfaces is not considered in this study and therefore the second term in the J integral is disappeared. The J integral can be transformed to a domain integral with the divergence theorem [50]

$$J = \int_A \left(\frac{\partial}{\partial x}\right) \cdot (H \cdot \bar{q})\ dA \tag{2.38}$$

where A is the area domain enclosed by the closed contour, and dA the infinitesimal area segment. By using the equilibrium equation,

$$\left(\frac{\partial}{\partial x}\right) \cdot \sigma + f = 0 \tag{2.39}$$

and the gradient of the strain energy for a homogeneous material with constant material parameters,

$$\frac{\partial W\left(\epsilon^m\right)}{\partial x} = \frac{\partial W}{\partial \epsilon^m} : \frac{\partial \epsilon^m}{\partial x} = \sigma : \frac{\partial \epsilon}{\partial x} \tag{2.40}$$

the 2D J-integral can be rewritten as [50]

$$J = -\int_A \left[H : \frac{\partial \bar{q}}{\partial x} + \left(f \cdot \frac{\partial u}{\partial x}\right) \cdot \bar{q}\right] dV \tag{2.41}$$

where ϵ^m is the mechanical strain and f is the body force per unit volume.

The 3D calculations are performed in a similar manner as the two 2D case, but the energy release rate is initially calculated with respect to finite extension of crack front, denoted by $\bar{J}$. This is then used to calculate the point-wise energy release rate $J\left(s\right)$ for each nodes along the crack tip. This procedure is done by defining a parametric variable s along the crack front with a local coordinate system. The local Cartesian coordinate system is set up at the crack front with respect to s as seen in Figure 2.10. The axis, x_3, runs tangentially to the crack, x_2 is defined perpendicular to the crack plane, and x_1 normal to the crack front. x_1 together with x_2 creates a plane perpendicular to the crack front. Hence, $J\left(s\right)$ is described in the x_1x_2 plane.

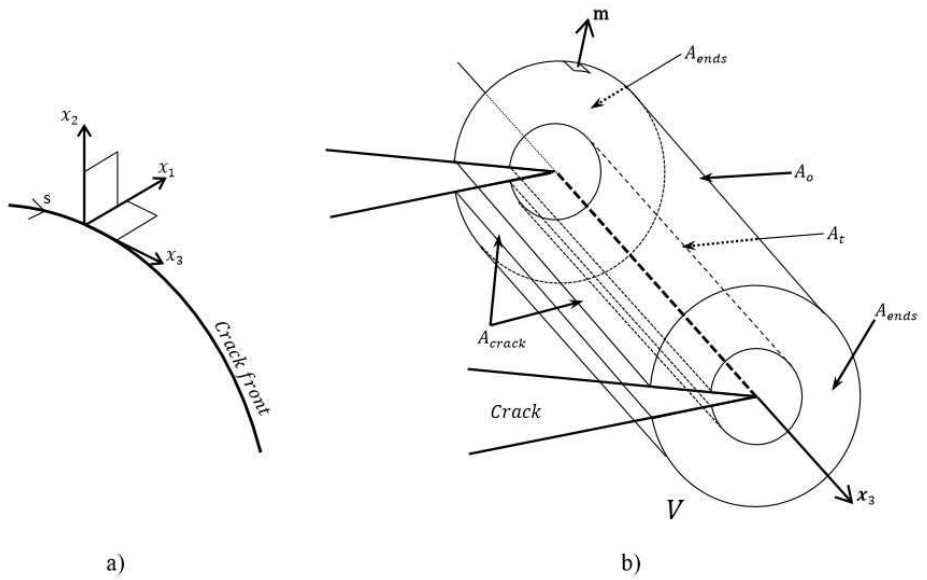

Figure 2.11: a) Local coordinate system for s. b) Contours for 3D crack front.[14]

In 3D, the energy release for a unit segment of crack extension over a finite segment of the crack front, $\bar{J}$, is defined as [50]

$$\bar{J} = -\int_V \left[H : \frac{\partial \bar{q}}{\partial x} + \left(f \cdot \frac{\partial u}{\partial x} \right) \cdot q \right] dV \tag{2.42}$$

where H, f and u are defined as before but in 3D. The weighting function $\bar{q}$ is defined for the various surfaces. The point-wise J integral, $J\left(s\right)$, for a general 3D crack front is calculated by dividing with the increase of the crack area due to the crack extension for the finite segment. The 3D case is a volume integral for the domain V shown in Figure 2.11 which is a tubular domain for a closed contour along a finite segment of the crack front. The 3D surface integral consists of $A_t, A_o, A_{cracks}, A_{ends}$. represented in Figure 2.11.

The SIF's K_I, K_{II}, K_{III} are used in LEFM to represent the local stress field at crack tip. As stated in [14], SIF's are related to the J-integral through

$$J = \frac{1}{8\pi} K^T \cdot B^{-1} \cdot K \tag{2.43}$$

where $K = [K_I, K_{II}, K_{III}]^T$ and B is pre-logarithmic energy factor matrix which is diagonal for isotropic homogeneous material. Therefore, the expression for J integral given above simplifies to

$$J = \frac{1}{\bar{E}} \left(K_I^2 + K_{II}^2 \right) + \frac{1}{2G} K_{III}^2. \tag{2.44}$$

In here $\bar{E} = E$ for plane stress and $\bar{E} = \frac{E}{1-\nu^2}$ for plain strain, axisymmetry and three dimensions.

As stated in [14], the J-integral for a given problem can be written as

$$J = \frac{1}{8\pi} K_I B_{11}^{-1} K_I + 2K_I B_{12}^{-1} K_{II} + 2K_I B_{13}^{-1} K_{III} + (terms\ without\ K_I) \quad (2.45)$$

The J-integral for an auxiliary field, Mode I crack tip field with k_I as stress intensity factor, is chosen as

$$J_{aux} = \frac{1}{8\pi} \left(k_I \cdot B_{11}^{-1} \cdot k_I \right). \quad (2.46)$$

Superposition of the auxiliary field and the real field gives

$$J_{tot}^I = \frac{1}{8\pi} \left[(K_I + k_I) B_{11}^{-1} ((K_I + k_I) + 2 (K_I + k_I) B_{12}^{-1} K_{II} + 2 (K_I + k_I) B_{13}^{-1} K_{III} \right]. \quad (2.47)$$

The interaction integral can be expressed as

$$J_{int}^I = J_{tot}^I - J_{aux}^I - J = \frac{k_I}{4\pi} \left(B_{11}^{-1} K_I + B_{12}^{-1} K_{II} + B_{13}^{-1} K_{III} \right). \quad (2.48)$$

The same procedure is done for Mode II and Mode III. The equations for the three modes can be written as

$$J_{int}^\alpha = \frac{k_\alpha}{4\pi} B_{\alpha\beta}^{-1} K_\beta. \quad (2.49)$$

Choosing unit values for k_α, the stress intensity factors are expressed in terms of the interaction integral as

$$K = \frac{1}{4\pi} B \cdot J_{int} \quad (2.50)$$

where $J_{int} = \left[J_{int}^I, J_{int}^{II}, J_{int}^{III} \right]^T$. The interaction integral can be evaluated in a similar manner as the J-integral in for the three modes $\alpha = I, II, III$ including auxiliary stress and strain fields

$$J_{int}^\alpha = \lim_{\Gamma \to 0} \int_\Gamma n \cdot M^\alpha \cdot q \, d\Gamma \quad (2.51)$$

where M^α is given as

$$M^\alpha = \sigma : \epsilon_{aux}^\alpha I - \sigma \cdot \left(\frac{\partial u}{\partial x} \right)_{aux}^\alpha - \sigma_{aux}^\alpha \cdot \frac{\partial u}{\partial x}. \quad (2.52)$$

In here, aux denotes the auxiliary pure Mode I, Mode II and Mode III crack tip field for the corresponding Mode α.

2.7.2 Sensitivity of XFEM Solution to Element Size

XFEM in Abaqus supports only first order 3D solid continuum elements for stationary crack analysis as stated in previous section. The general purpose C3D8 linear brick element presented in Figure 2.12 is used throughout this study.

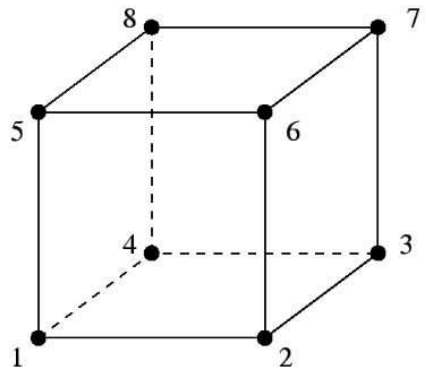

Figure 2.12: C3D8 brick element.

An initial study for mesh convergence for five different crack length is presented below. A Single Edge Notched Tension (SENT) specimen which has a width of 80 mm, length of 200 mm and thickness of 5 mm is considered for this study. The crack length (a) changes from 10 mm to 30 mm by an increment of 5 mm.

FE Model of the SENT specimen is illustrated in Figure 2.13. A uni-axial far field tension stress of 100 MPa is applied from the both ends of the specimen. The surface of the specimen is constrained in out of plane direction to create a plane strain condition.
K_I expression for plain strain condition is given as [41]

$$K_I = f\left(\frac{a}{w}\right)\sigma\sqrt{\pi a} \tag{2.53}$$

$$f\left(\frac{a}{w}\right) = 1.12 - 0.23\left(\frac{a}{w}\right) + 10.56\left(\frac{a}{w}\right)^2 - 21.74\left(\frac{a}{w}\right)^3 + 30.42\left(\frac{a}{w}\right)^4. \tag{2.54}$$

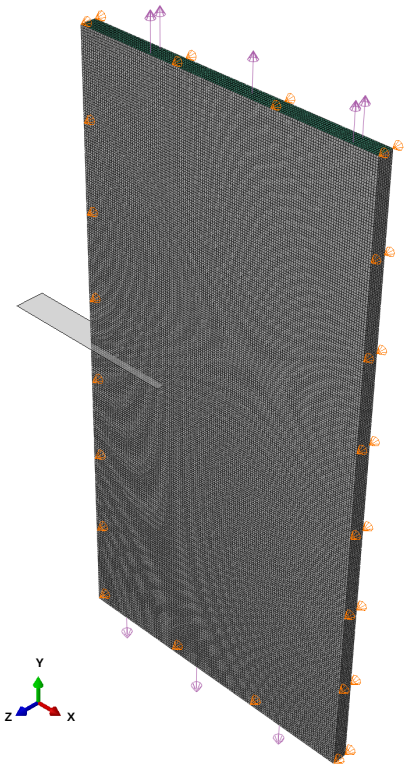

Figure 2.13: FE model for SENT specimen.

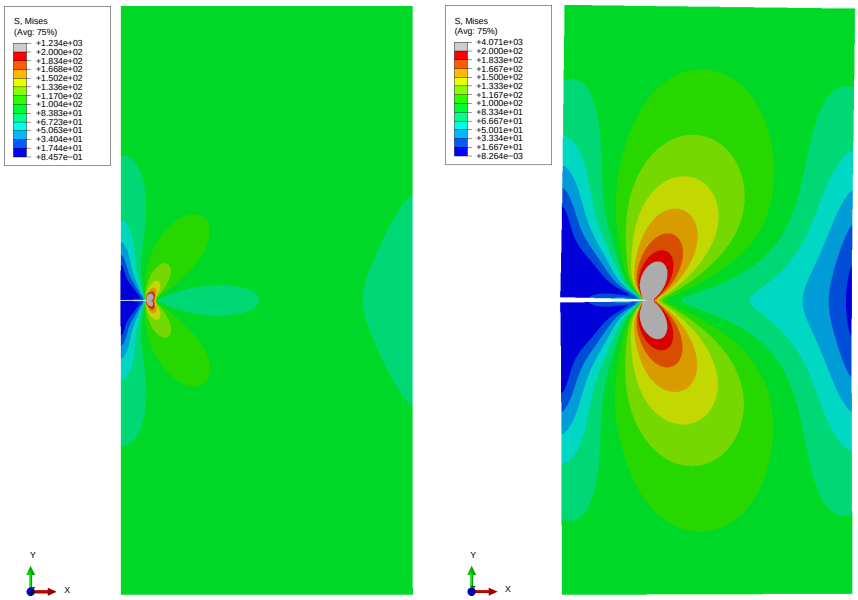

Figure 2.14: Von misses stress contour for SENT specimen.

Table 2.1: Effect of requested number of contours in XFEM

C1	C2	C3	C4	C5	C6	C7	C8	C9	C10	Average
2953	**1943**	1775	1719	1627	1664	1563	1608	1492	1583	1628.88
2870	**1824**	1734	1639	1657	1577	1533	1560	-	-	1616.67
2690	**1771**	1687	1637	1572	1543	-	-	-	-	1609.75
2514	**1687**	1613	1550	-	-	-	-	-	-	1581.50

Effect of requested number of contours is investigated by considering 4 to 10 contours by an increment of 2 on crack length a=30 mm by using a mesh size of 0.75 mm. The results are presented in Table 2.1. Cx in table stands for contour number. As stated in [14], Abaqus defines the contour domains in terms of element rings which surrounds the crack tip. By this explanation it is expected that the result of the first 4 contours will be the same when comparing the SIF values from different number of requested contours. But this case has not been observed. Moreover, the SIF results of the first two contours which are written in bold have a tendency to be higher than the remaining contours average as seen from presented results. The first two contours are discarded and the remaining contour values are averaged to make a fair calculation. Requesting eight contours gives the nearest value when compared to the analytical SIF (1612.3 MPa $\sqrt{\text{mm}}$).

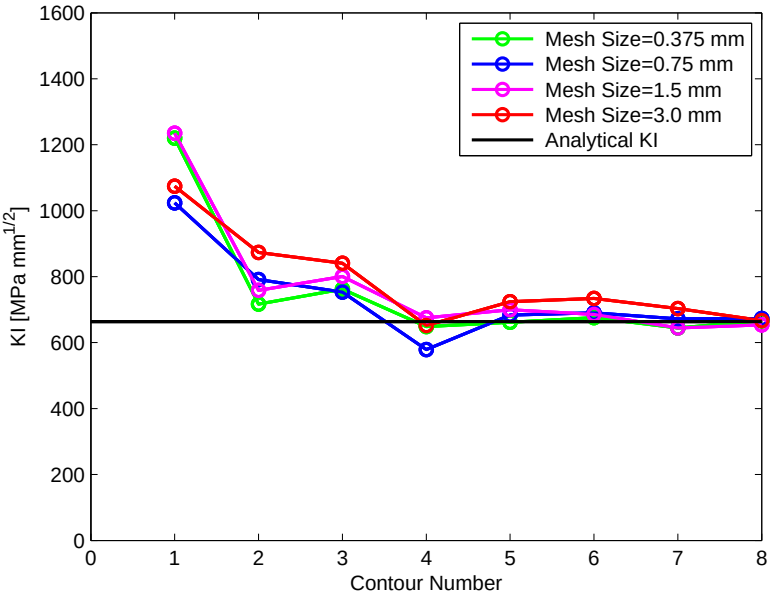

Figure 2.15: SIF results at 10 mm crack length for different element sizes.

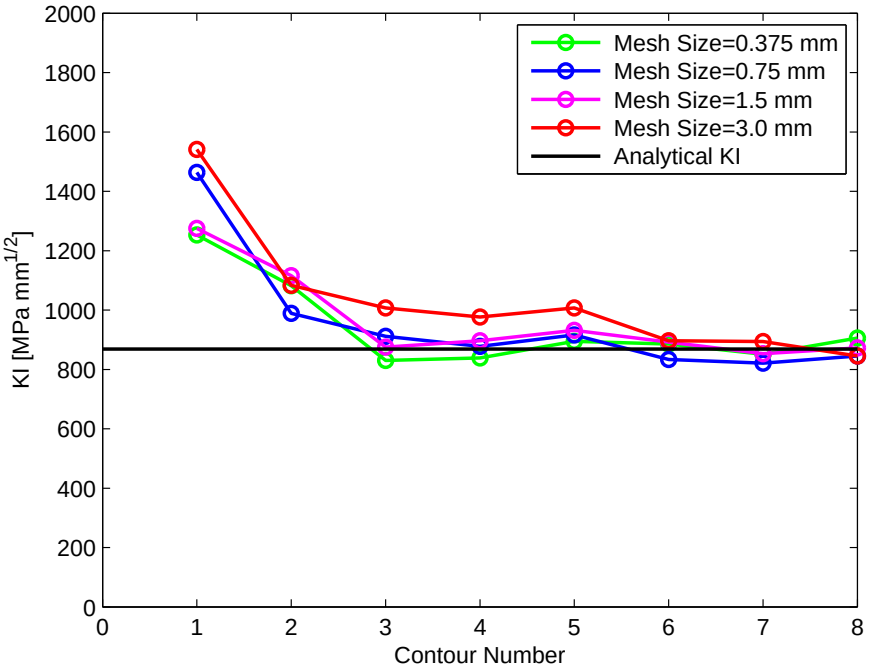

Figure 2.16: SIF results at 15 mm crack length for different element sizes.

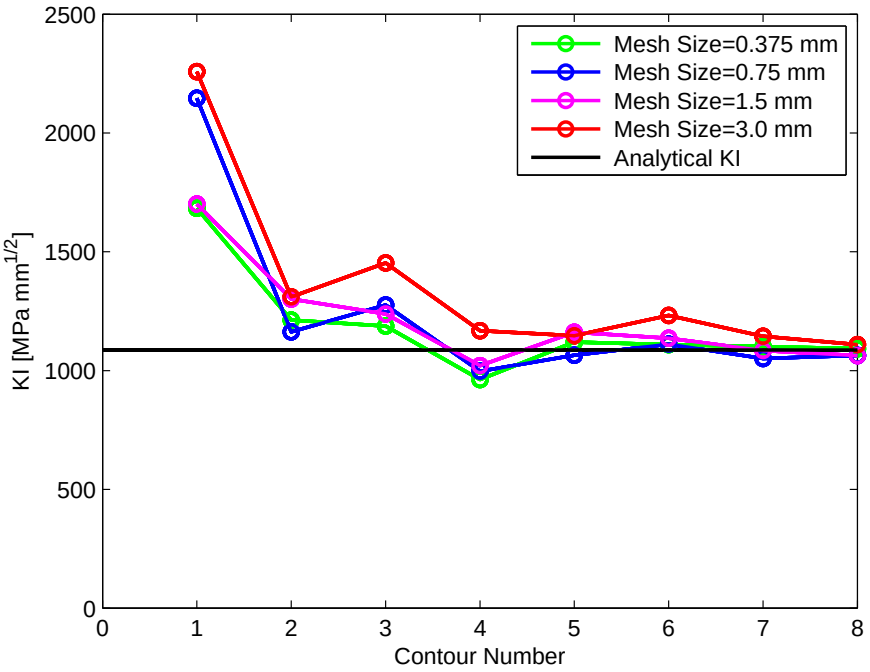

Figure 2.17: SIF results at 20 mm crack length for different element sizes.

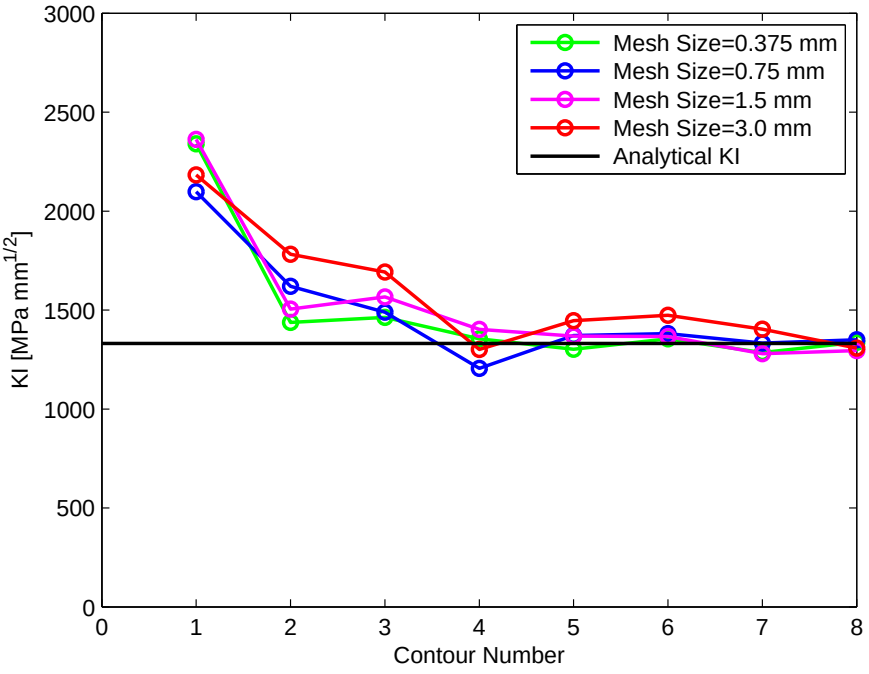

Figure 2.18: SIF results at 25 mm crack length for different element sizes.

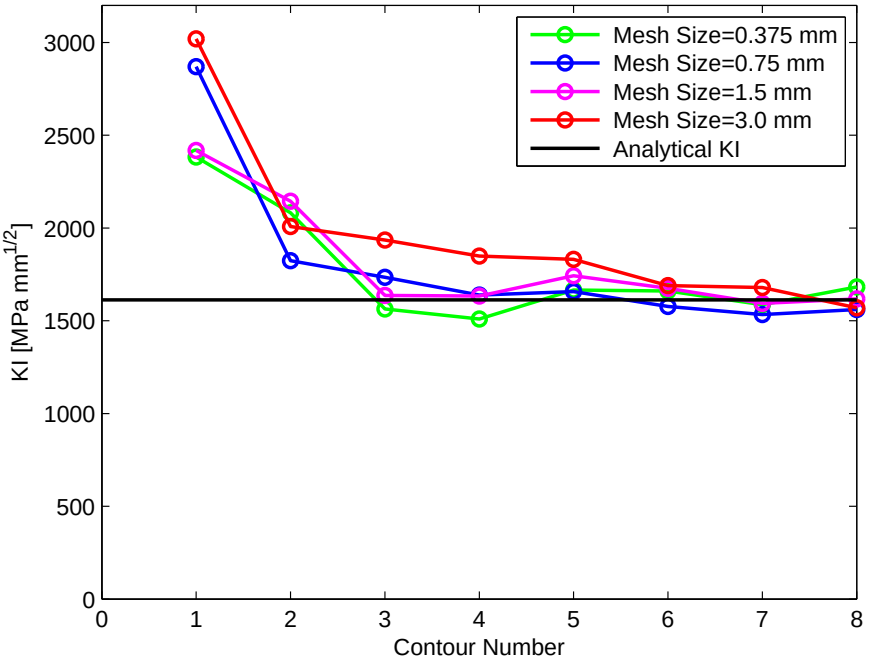

Figure 2.19: SIF results at 30 mm crack length for different element sizes.

Based on this study, eight contours requested in XFEM solutions for SIF calculations. In XFEM solutions four different mesh sizes are considered (0.375 mm, 0.75 mm, 1.5 mm, 3 mm) for each crack length. The SIF results from each contours for each crack length and mesh sizes are presented in Figures 2.15 through 2.19.

Averaged SIF values from last six contours are presented in Table 2.2 along with analytical SIF results and percentage error. As seen from the presented results in Table 2.2 for mesh sensitivity, the smaller the element size, the lower the error percentage.

Table 2.2: Mesh sensitivity of XFEM solutions for different crack length.

Mesh Size [mm]	**Crack Length [mm]**	**Analytical KI**	**KI_XFEM**	**% Error**
0.375	30	1612.3	1611.2	-0.07
0.75	30	1612.3	1616.7	0.27
1.5	30	1612.3	1649.8	2.32
3	30	1612.3	1759.0	9.10
Mesh Size [mm]	**Crack Length [mm]**	**Analytical KI**	**KI_XFEM**	**% Error**
0.375	25	1330.8	1349.5	1.41
0.75	25	1330.8	1344.8	1.05
1.5	25	1330.8	1379.5	3.66
3	25	1330.8	1437.3	8.01
Mesh Size [mm]	**Crack Length [mm]**	**Analytical KI**	**KI_XFEM**	**% Error**
0.375	20	1086.9	1095.2	0.77
0.75	20	1086.9	1094.0	0.66
1.5	20	1086.9	1117.3	2.80
3	20	1086.9	1208.8	11.22
Mesh Size [mm]	**Crack Length [mm]**	**Analytical KI**	**KI_XFEM**	**% Error**
0.375	15	868.5	867.7	-0.09
0.75	15	868.5	867.5	-0.11
1.5	15	868.5	886.8	2.10
3	15	868.5	937.8	7.98
Mesh Size [mm]	**Crack Length [mm]**	**Analytical KI**	**KI_XFEM**	**% Error**
0.375	10	663.6	676.4	1.94
0.75	10	663.6	675.2	1.76
1.5	10	663.6	693.1	4.45
3	10	663.6	720.0	8.50

Some recommendations are given based on this study.

- Perform a mesh sensitivity study and determine the mesh size which does not change the results by further refinement. Choose a reasonable mesh size by this way. As seen from Table 2.2, there is no such a big change by mesh refinement in XFEM solutions after a reasonable mesh size. In coarse mesh sizes relative error is much higher. Further refinements might be unnecessary after a reasonable mesh size since it increases the computational time.
- Discard the first two contours which are far away from actual value. Honestly, take the average value of the remaining contours. It is advisable to discard only the first contour if a small number of contours are requested. Requesting eight contours by excluding the first two is recommended.
- It is also recommended that if there is any value which is far away from the average value omit these values as well.

CHAPTER 3

COMPUTATIONAL ALGORITHM

In this study, an automatic fatigue crack propagation and life determination algorithm is developed which can propagate both edge and internal cracks under mode I and mixed mode loading conditions. This algorithm uses the capability of modelling stationary cracks of Abaqus software in order to model propagating cracks. In this algorithm, a Fortran script which calls Abaqus for each incremental crack growth analysis step is used for determination of SIF's and crack growth direction from Abaqus solutions. Analytical FCG life calculations under user defined loading spectra are performed by considering the load history effects by using appropriate retardation models presented in section 2.5. Before the script automatically propagates the crack, one has to provide an input file of modelled initial stationary crack in Abaqus environment in a file with .py extension which is used by Abaqus to construct the analysis model in each step of crack tip update. At the end of each analysis step Fortran script reads the SIF values from Abaqus result file. The script automatically calculates the crack growth rate (da/dN) through Nasgro equation presented in (2.11) for each loading cycle available in user defined load spectrum. Crack growth at each cycle is summed up until the total crack growth amount reached a predetermined value. This predetermined value can be set by user to lessen the number of analysis. But, it should be small enough for the correct crack path and life prediction. Direction of crack growth is determined by $K_{II} = 0$ criterion which is already implemented in Abaqus. The script updates the crack tip by calculating the new crack tip coordinates after the predetermined crack growth increment is reached. Crack growth analysis is carried out by this algorithm until calculated SIF values exceed the critical SIF. The main structure of the developed FCG algorithm is presented in Figure 3.1.

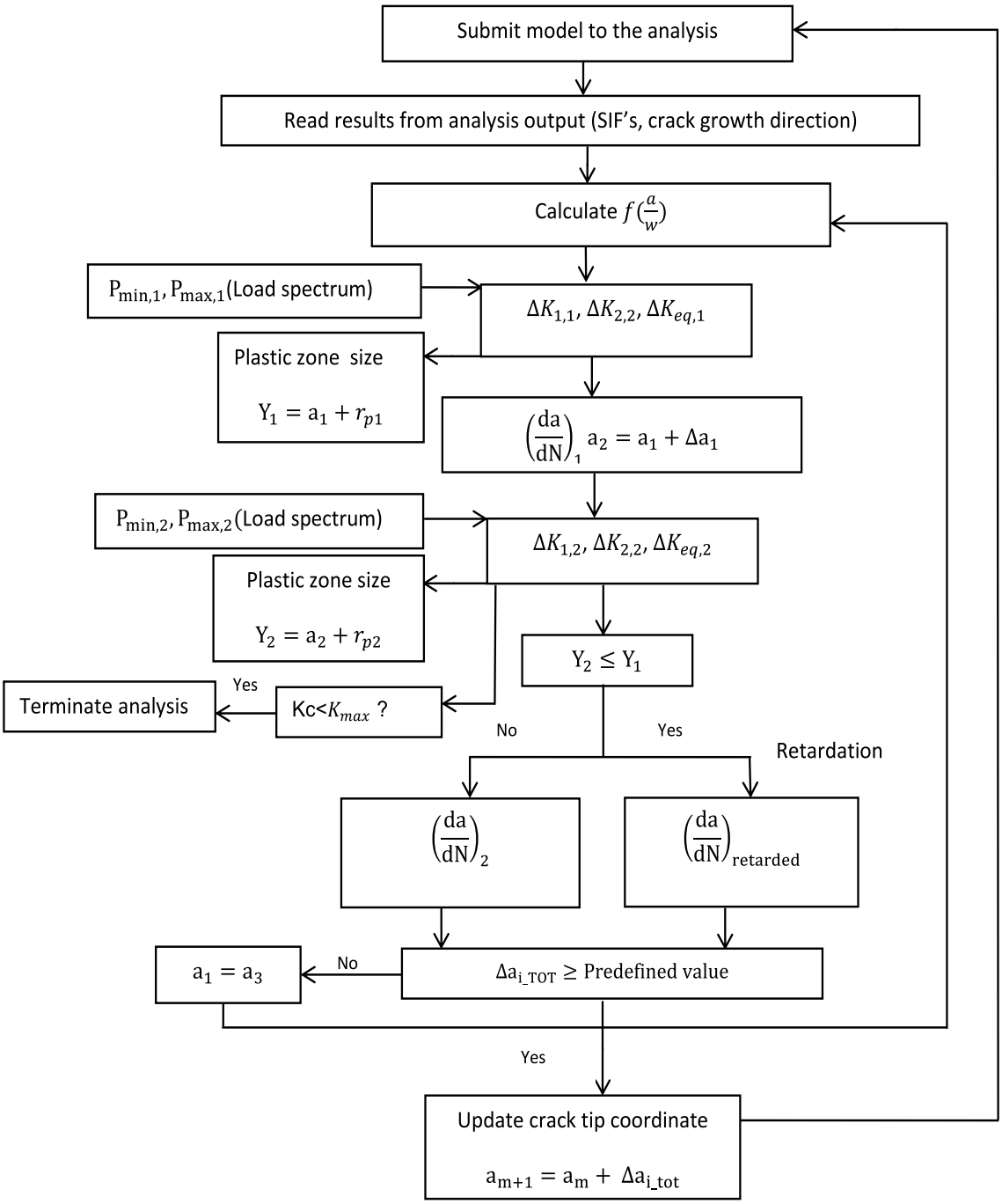

Figure 3.1: FCG algorithm flowchart.

A simple schematic representation of crack updating is illustrated in Figure 3.2, where θ is the crack growth direction and (x_i, y_i) is the crack tip coordinates at i^{th} cycle.

$$x_{i+1} = x_i + \Delta a cos(\theta) \tag{3.1}$$

$$y_{i+1} = y_i + \Delta a sin(\theta) \tag{3.2}$$

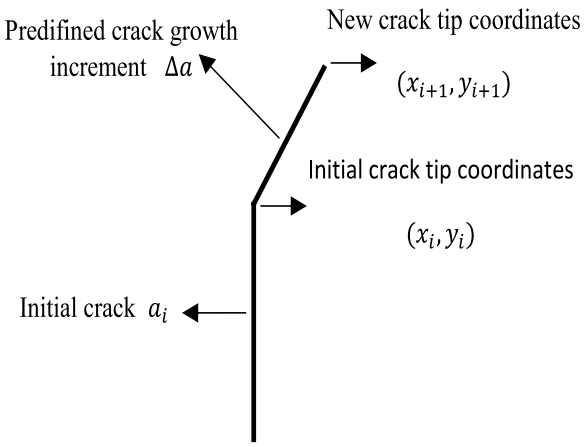

Figure 3.2: Crack tip update procedure.

The procedure for each successive step can be described in detail as follows.

Step1. The FCG algorithm starts with initial inputs; FCG rate equation constants, retardation model parameters, initial crack length and initial crack tip coordinates. For the first analysis step the code needs an initial input file which contains the definition of initial stationary crack modelled by XFEM in Abaqus environment. This main input file must also contain the finite element mesh, model boundary conditions and dummy load on the model. The initial model is submitted to the FE solver and the code stand idle until the analysis end. At the end of analysis, script reads the SIF values on the node located at mid point of the specimen thickness from the previous analysis outputs. Fortran script calculates the correction factor $f(a/w)$ by using this SIF value obtained under the loading on the model through general SIF expression, $K = f(a/w)\sigma\sqrt{\pi a}$. The load on the model can be set by the user since the further SIF calculations performed by using the linear relation between load and SIF.

Step2. The script automatically calculates the crack growth rate $\left(\frac{da}{dN}\right)$ for each cycle defined in external spectrum file. If an OL or UL is detected in the spectrum, retardation effect are taken into account in crack growth rate by using a retarded crack growth rate formulation $\left(\frac{da}{dN}\right)_{ret,i}$. The calculated crack growth at each cycle is summed until the total crack growth reached a predetermined value.

Step3. When the predetermined crack growth increment is reached, the script calculates the new crack tip coordinates by using crack growth direction extracted from result file. After performing the calculation of new crack tip coordinates, the script

writes the new crack tip coordinates to the its location in crackupdate.py file. Crack-update.py file is exported to the main script to update the XFEM crack in Abaqus. By this way, in next step of analysis the model recognize the updated crack as new XFEM crack and solve the updated model. The same procedure is followed by this way. This analysis procedure is carried out until the calculated SIF values exceed the critical SIF or a desired level by the user.

CHAPTER 4

MODEL VERIFICATION WITH EXPERIMENTAL RESULTS

In this study, validation of developed computational FCG algorithm is demonstrated by a series of experimental results reported in [51, 52, 53, 54]. Details of simulated specimens, comparisons of predicted FCG path and life with experimental results are presented from section 4.1 to 4.4. FCG simulations for all case studies are presented through 3D hexahedral elements (C3D8). Mesh convergence studies are carried out before each analysis to ensure that appropriate element size and predetermined crack growth increment values are used. XFEM results are almost insensitive to the mesh refinements after a reasonable mesh size as demonstrated in Chapter II and in literature studies (see e.g. [53, 55]). In XFEM simulations, the mid-side node through the thickness direction of the specimen is considered for SIF calculations. Model with initial crack is created in Abaqus environment and analysis input file is submitted to automatic crack growth script. The rest of the analysis completed by automated crack growth script.

4.1 FCG Life and Path Under Mode I Loading

The experimental study, on internal through cracked specimen conducted by Porter [51] on $7075 - T6$ aluminium alloy specimen is used for the purpose of proving the capability of the developed algorithm in estimation of crack growth life and path under variable amplitude loading conditions in uni-axial mode I loading. The material properties are as follows: elastic modulus, $E = 69.6$ GPa, Poisson's ratio $\nu = 0.33$ and yield stress $\sigma_y = 520$ MPa. The specimen has a width of 305 mm, length of 915

mm, thickness of 4.1 mm and an initial crack size of (2a) 12.7 mm. The geometry of the specimen is shown in Figure 4.1. The FE model is also presented in Figure 4.2.

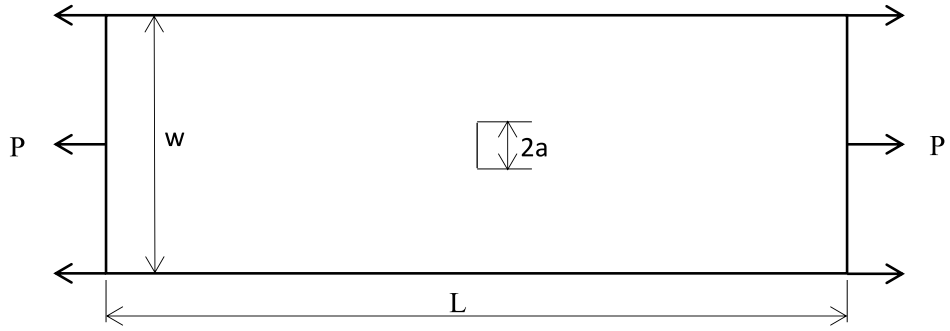

Figure 4.1: Geometry of internal cracked specimen [51].

A mesh size of 0.4 mm is used in simulations. Predefined crack growth increment is considered as 2 mm. Modified Generalized Willengborg retardation model presented in (2.25)-(2.27) are used in this series of simulations to accounts for the retardation effect caused by OL and OL-UL.

Figure 4.2: FE model of internal cracked specimen.

The analytical SIF solution for center cracked specimen under mode I loading is expressed as

$$K_I = \frac{P}{wt}\sqrt{\pi a} f\left(\frac{a}{w}\right) \tag{4.1}$$

where, t and w are the thickness and width of the specimen, P is the applied axial load and $f\left(\frac{a}{w}\right)$ is the geometry correction factor which depends on crack length to specimen width ratio and given in [41] as

$$f\left(\frac{a}{w}\right) = \sqrt{sec\frac{\pi a}{w}}. \tag{4.2}$$

Nasgro material parameters C and n are calibrated according to CAL test result. Other parameters are used as proposed by Nasgro material database and presented in Table 4.1.

Table 4.1: Nasgro equation constants for Al 7075-T6 internal cracked plate[2].

ΔK_{th}	ΔK_{ic}	C	n	p	q	S_{max}/σ_0	α
$80MPa\sqrt{mm}$	$730MPa\sqrt{\text{mm}}$	9.8610^{-12}	2.9	0.5	1	0.3	2.0

Schematic representations of the loading spectra used in FCG analysis are given in Figures 4.3 and 4.4.

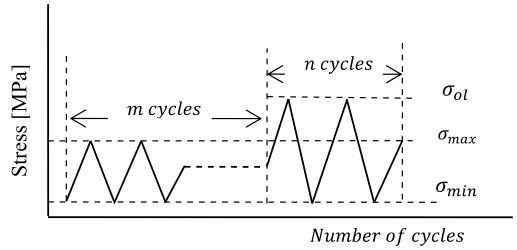

Figure 4.3: Block of OL spectrum for internal cracked specimen.

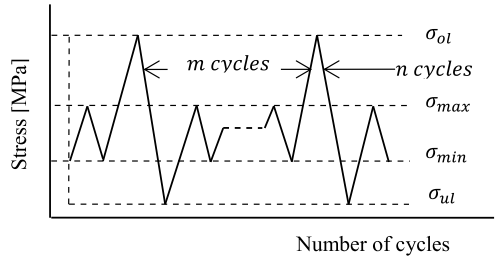

Figure 4.4: Block of OL-UL spectrum for internal cracked specimen.

Table 4.2: Load spectra for Al 7075-T6 internal cracked specimen [51].

Spectrum No	$\sigma_{min}[MPa]$	$\sigma_{max}[MPa]$	$\sigma_{ol}[MPa]$	$\sigma_{ul}[MPa]$	m	n
Spectrum 1	3.45	68.95	—-	—-	CAL	CAL
Spectrum 2	3.45	68.95	76.54	—-	29	1
Spectrum 3	3.45	68.95	103.43	—-	29	1
Spectrum 4	3.45	68.95	103.43	—-	50	1
Spectrum 5	3.45	68.95	103.43	—-	300	1
Spectrum 6	51.72	103.43	155.14	31.03	50	1
Spectrum 7	51.72	103.43	155.14	5.17	50	1

A total of seven different loading spectra which are presented in Table 4.2 are used in XFEM FCG simulations. The same simulations were also conducted by using Nasgro software to compare the resulting FCG life under defined loading spectra. In this preliminary study only K_I is considered since K_{II} always zero through crack length. The results obtained from XFEM based automatized algorithm, Nasgro software and experiments presented by Porter [51] were compared with each other and presented in Figures 4.5 through 4.11.

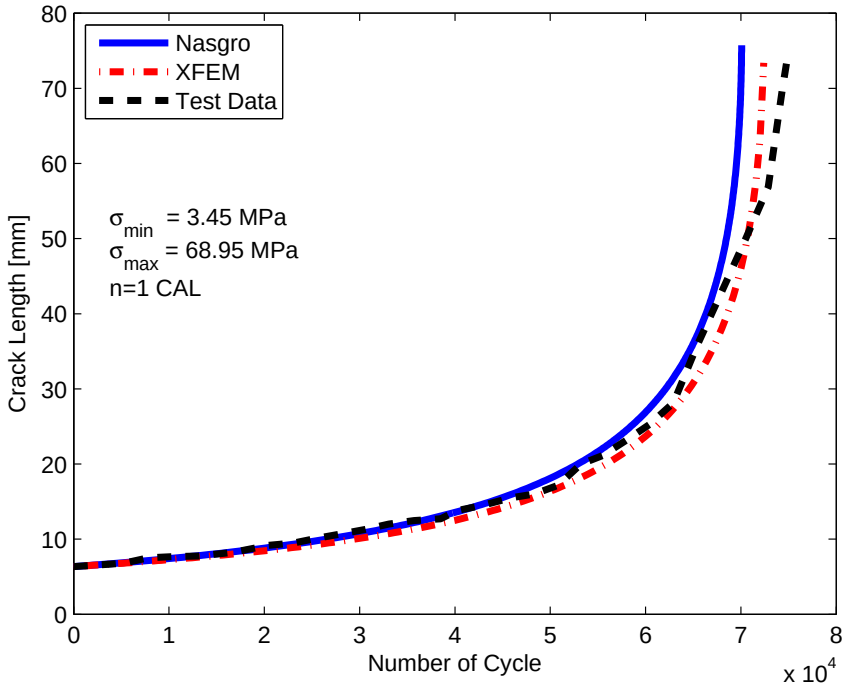

Figure 4.5: Comparison of FCG life for constant amplitude loading.

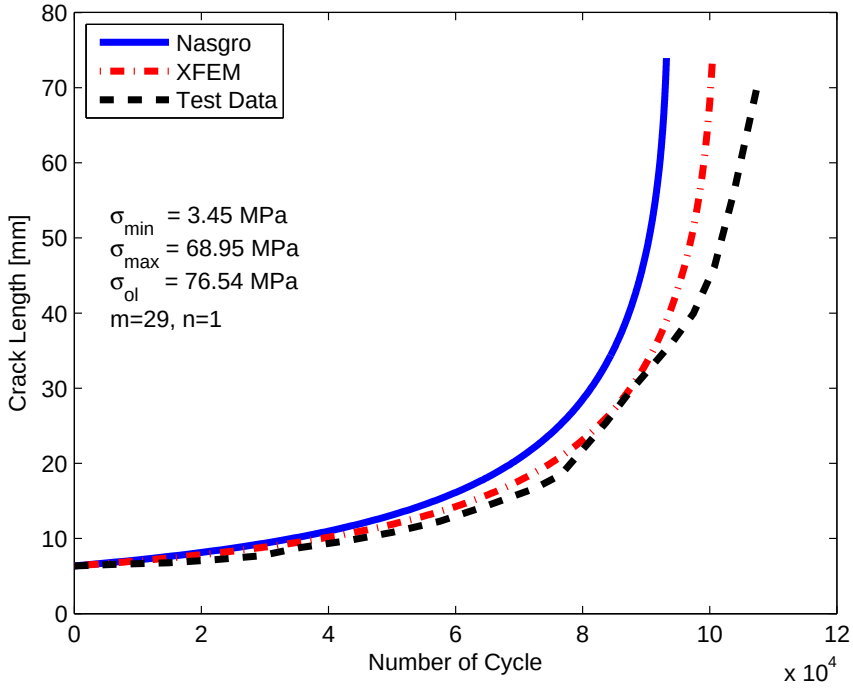

Figure 4.6: Comparison of FCG life for spectrum 2.

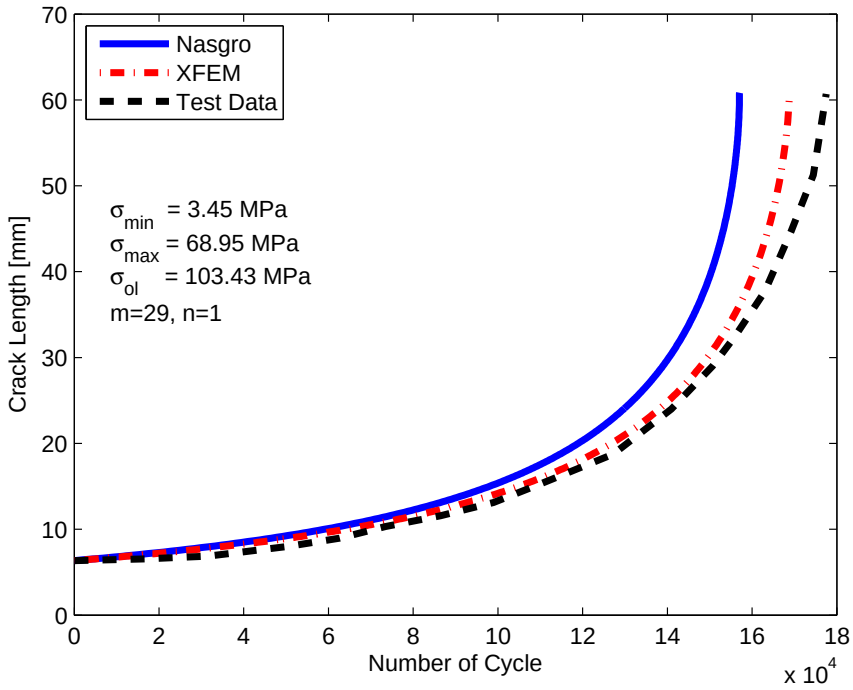

Figure 4.7: Comparison of FCG life for spectrum 3.

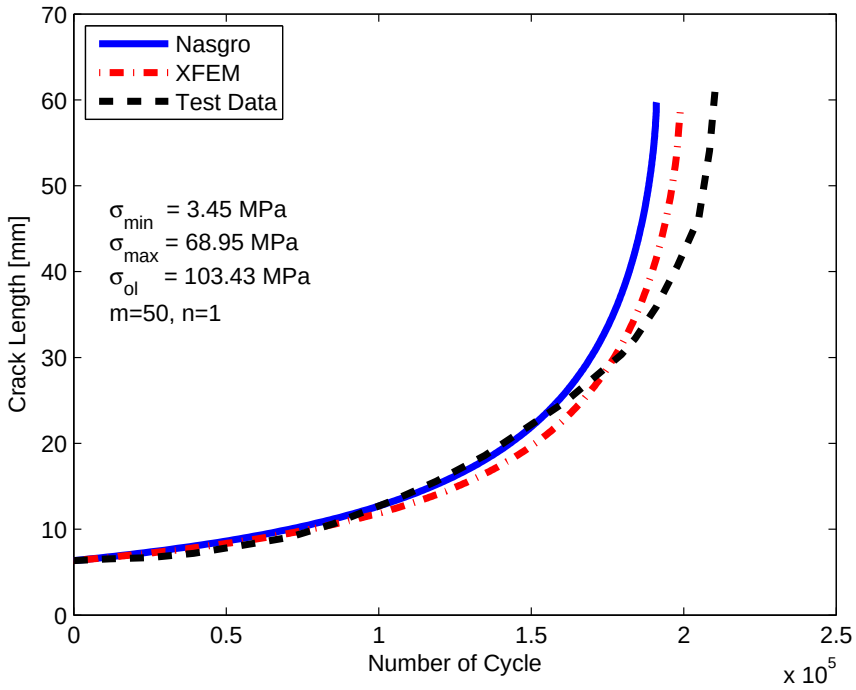

Figure 4.8: Comparison of FCG life for spectrum 4.

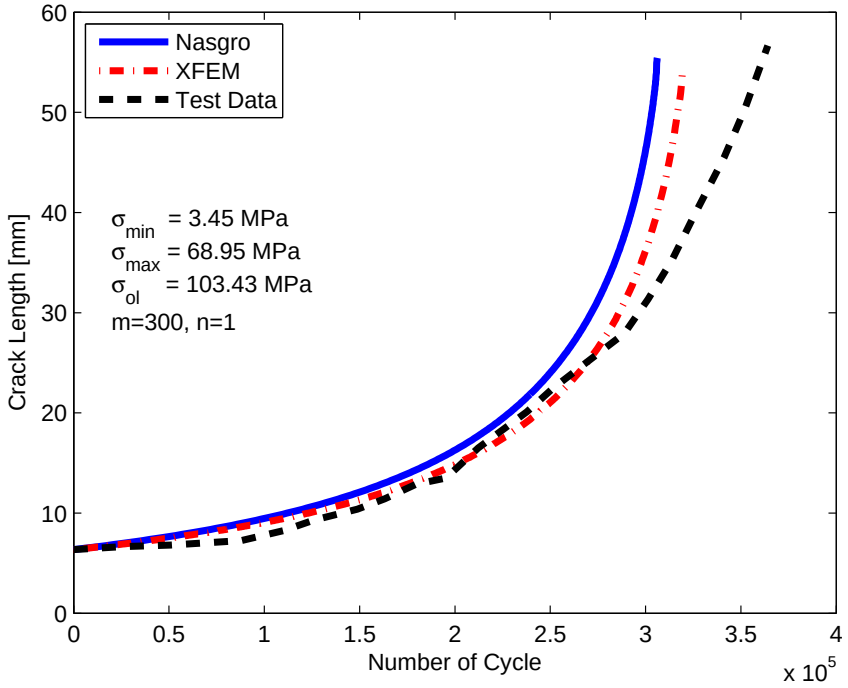

Figure 4.9: Comparison of FCG life for spectrum 5.

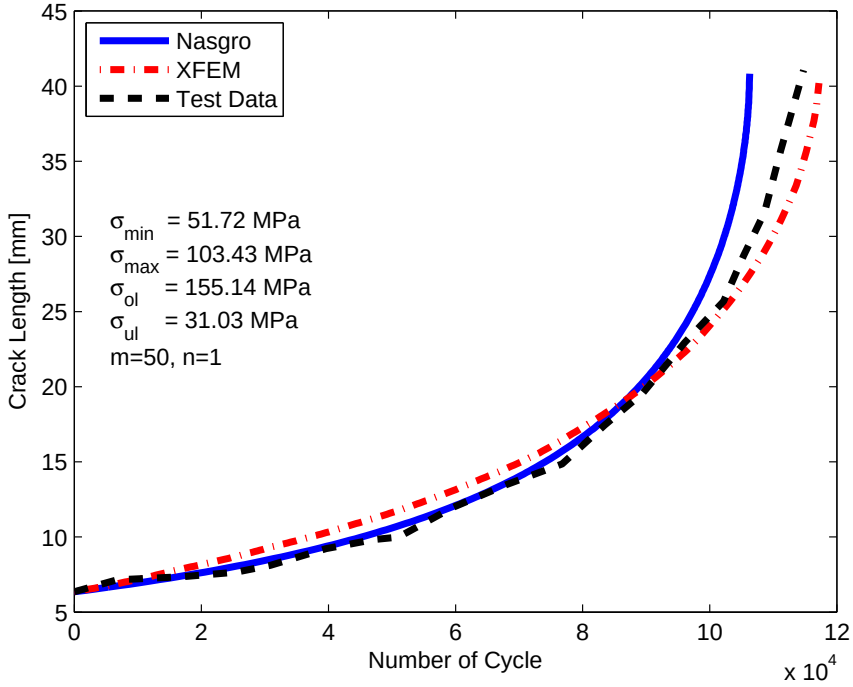

Figure 4.10: Comparison of FCG life for spectrum 6.

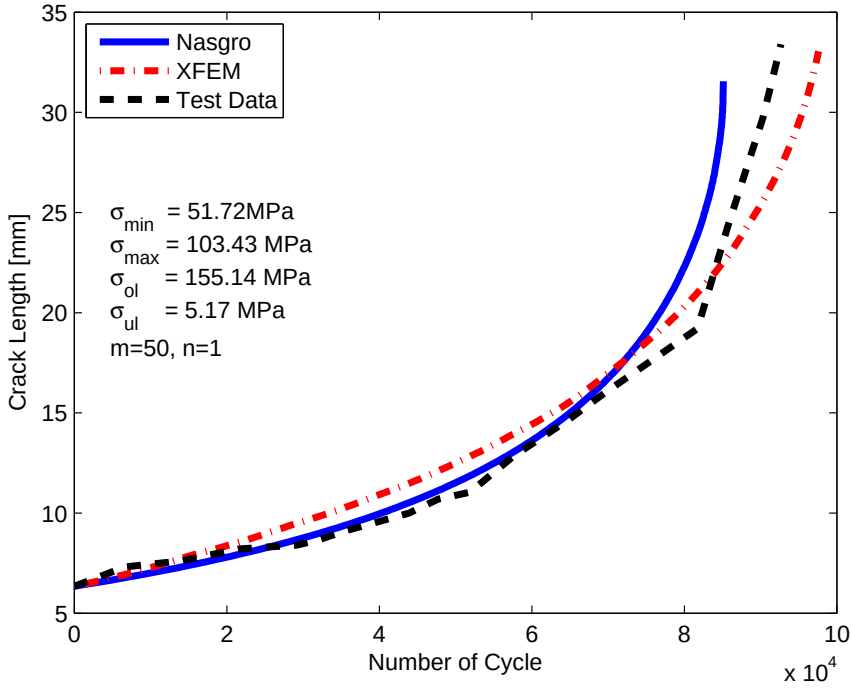

Figure 4.11: Comparison of FCG life for spectrum 7.

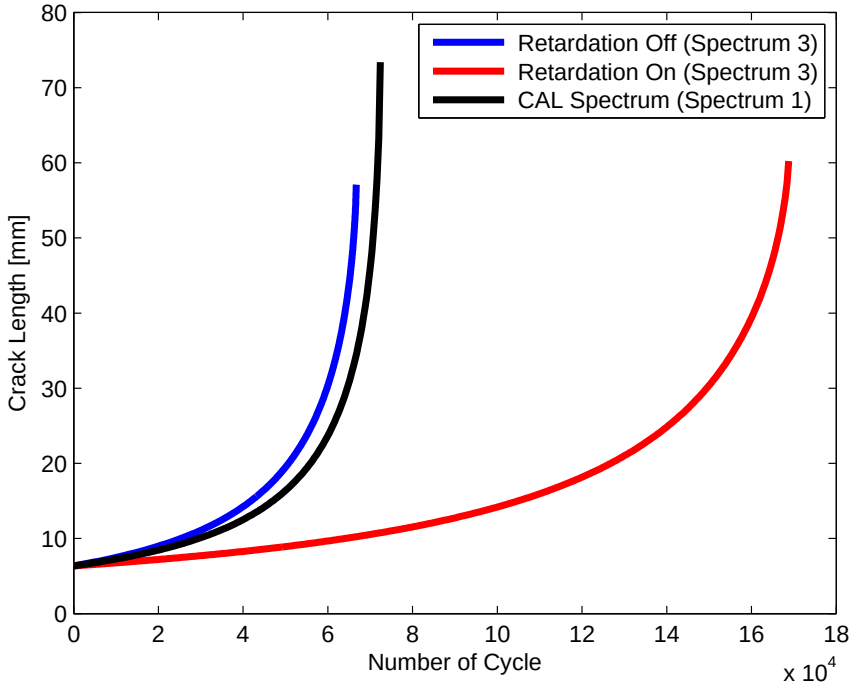

Figure 4.12: Retardation on-off for spectrum 3.

In order to show the importance of the retardation effect in the calculations, an analysis is performed for spectrum 3 without taking into account the retardation effect. As seen from Figure 4.12, spectrum 3 resulted with a shorter FCG life than CAL spectrum (spectrum 1) due to effect of periodic OL. Incorporating the retardation effect to the calculations has been seen to be lengthened the FCG life by a great amount.

As seen from presented Figures 4.5 through 4.11, FCG life results agree with Nasgro and test data with some minor discrepancies related to material and test data. By these series of simulations, the capability of the developed computational algorithm proven to be reliable in mode I loading in terms of crack path evaluation and FCG life predictions by accounting the load history effect. It is obvious that neglecting load history effect of in FCG life calculations under VAL can lead to completely invalid life predictions.

The effect of OL spacing and amplitude can also be seen in presented figures. The retardation effect is better observed in the case of OL applied at large intervals since in the case of small intervals a new OL is applied before the retardation effect is over.

Another remark is that, in the case of higher OL levels the retardation effect is also higher, due to the fact that, the larger the OL means higher yield zone region and consequently higher the delay effect on crack growth rate in subsequent load cycles. However, this is valid up to a certain level of OL. Very high OL can lead to sudden acceleration and failure of the components.

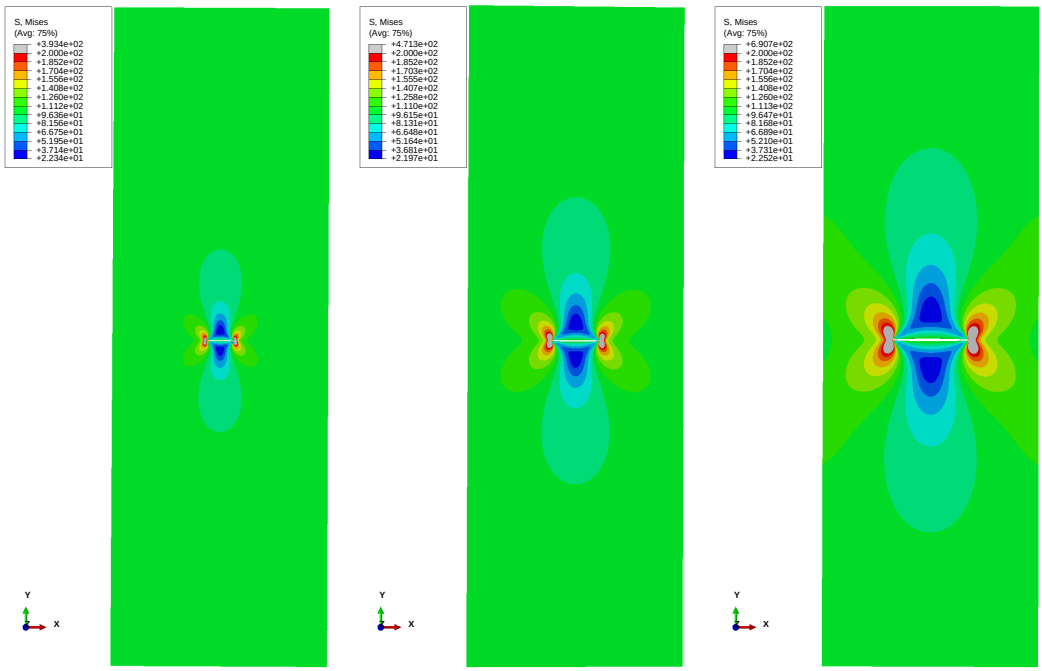

Figure 4.13: Crack growth path for internal cracked specimen.

The resulting crack growth path from Abaqus simulation along with Von misses stress distribution is presented in Figure 4.13. Since the simulated specimen is under the action of uni-axial mode I loading, the crack propagates straightly in the direction perpendicular to the loading as expected.

The case studies under mixed mode conditions which is the main purpose of the undertaken study are presented in the following sections.

4.2 Crack Path Under Mixed Mode Monotonic Load

In this case study, crack path evaluation capability of proposed algorithm under mixed mode condition has been validated for different initial crack lengths and crack locations in polymethyl methacrylate (PMMA) beam given in Figures 4.14 and 4.15 without and with holes configurations respectively. Available experimental results presented in [52] are used for the verification of simulated crack paths.

The loading acts on top mid-span location of the specimen and is a monotonic load of 100 kN . The simulated beam has a length of $2L = 508$ mm, a width of $w = 203.2$ mm and thickness of $t = 12.7$ mm. The overall dimensions, hole locations and hole sizes for all specimens are the same. Crack location and crack length differ for each specimens. For the first configuration, the initial crack has a length of $a_0 = 25.4$ mm and located at distance of $d = 152.4$ mm from the mid-span of the beam. The second configuration differs from the first one in terms of initial crack length of $a_0 = 63.5$ mm. The third configuration differs from the first one in terms of initial crack length of $a_0 = 38.1$ and also initial crack location, which is located at a distance $d = 127$ mm from mid-span of the beam. The material properties are assumed as elastic modulus of $E = 205$ GPa and Poisson's ratio of $\nu = 0.3$.

This case study is conducted for the purpose of testing the crack path prediction capability of the algorithm in mixed mode loading condition. By using the developed algorithm, angles of the crack extension and positions of the crack tip have been determined for each crack increments. Each of three specimens was simulated with and without hole configurations as presented in Table 4.3.

Comparison of experimental and simulated crack tip coordinates for all specimen configurations are presented in Figures 4.22 through 4.27. The last step of crack propagation paths from Abaqus simulations for each specimens along with Von misses stress contours are also presented in Figures 4.28 through 4.33.

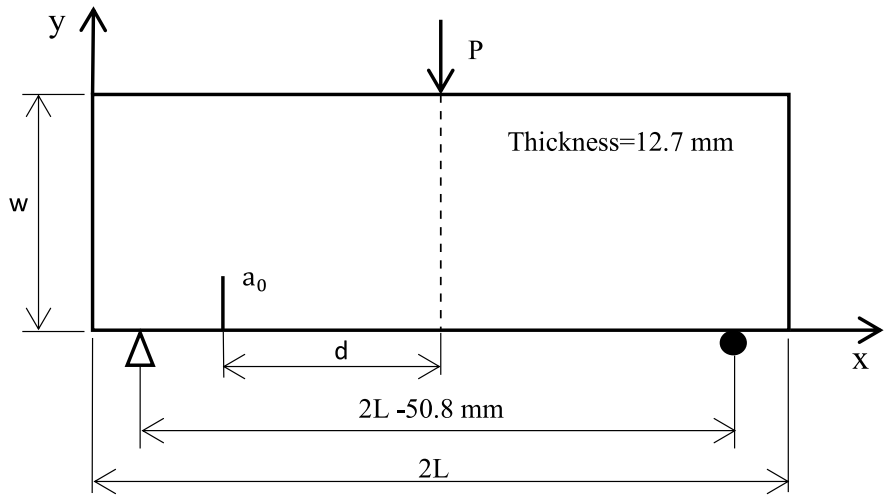

Figure 4.14: Geometry of PMMA beam without hole configuration [52].

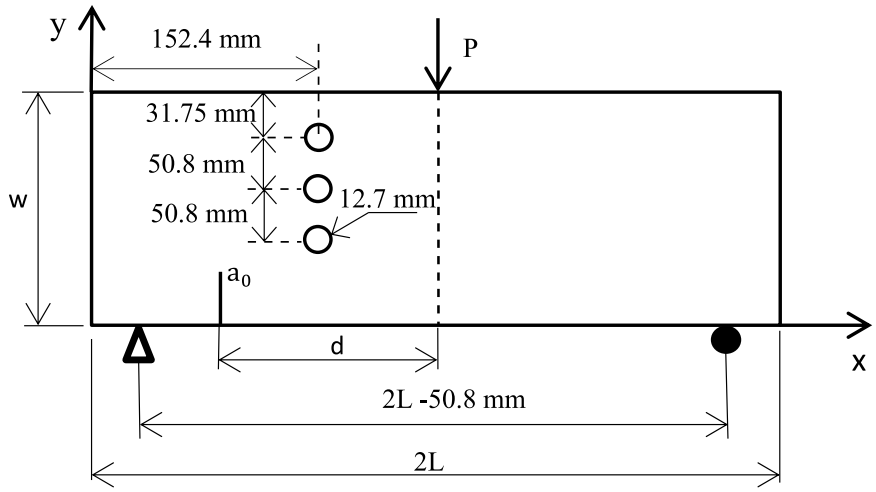

Figure 4.15: Geometry of PMMA beam with holes configuration [52].

Table 4.3: Simulated PMMA beam configurations.

Specimen No	Crack length a[mm]	Crack location d[mm]	Hole Configuration
1	25.4	152.4	Without holes
2	25.4	152.4	With holes
3	63.5	152.4	Without holes
4	63.5	152.4	With holes
5	38.1	127	Without holes
6	38.1	127	With holes

Initial FE models for specimens are presented in Figures 4.16 and 4.17. Specimens are constrained from left pin locations in all degrees of freedom as in the case of experiments and only first translational degree of freedom u_x is unconstrained in right pin location. The plate is under the action of a concentrated load (100 kN) which acts on the top mid-span location.

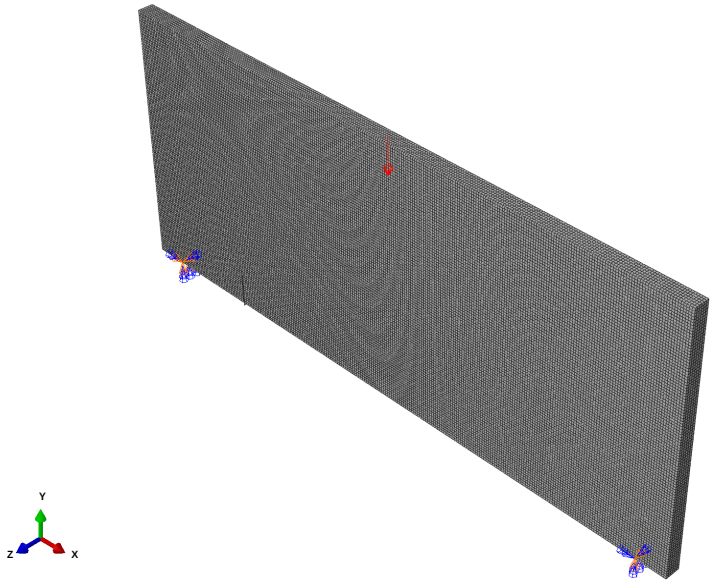

Figure 4.16: FE model for PMMA beam without hole configuration.

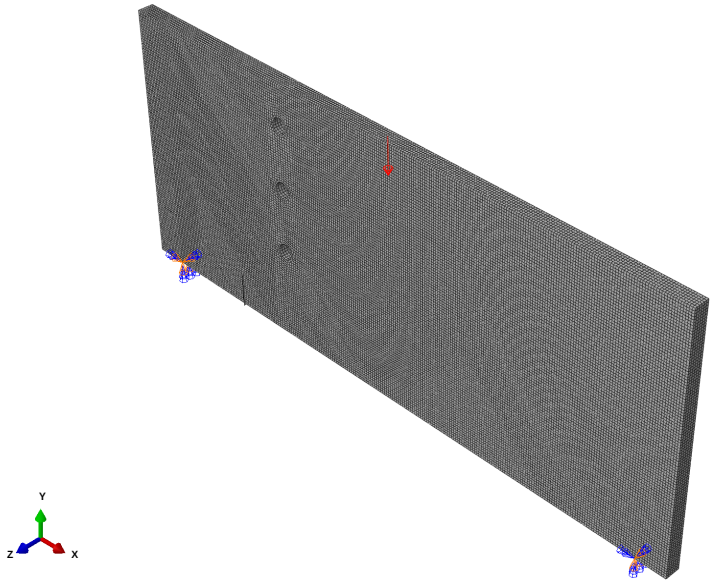

Figure 4.17: FE model for PMMA beam with holes configuration.

The effect of mesh density on crack path is investigated on specimen 2. Two different mesh configurations (Mesh 1= 2 mm, Mesh 2=1 mm) are used in simulations with a crack growth increment of 12.7 mm. Simulated crack paths with two different mesh configurations along with experimental crack path is presented in Figure 4.18 in a close view. There is no big difference between crack path but finer mesh has better agreement with experimental result as seen from Figure 4.18.

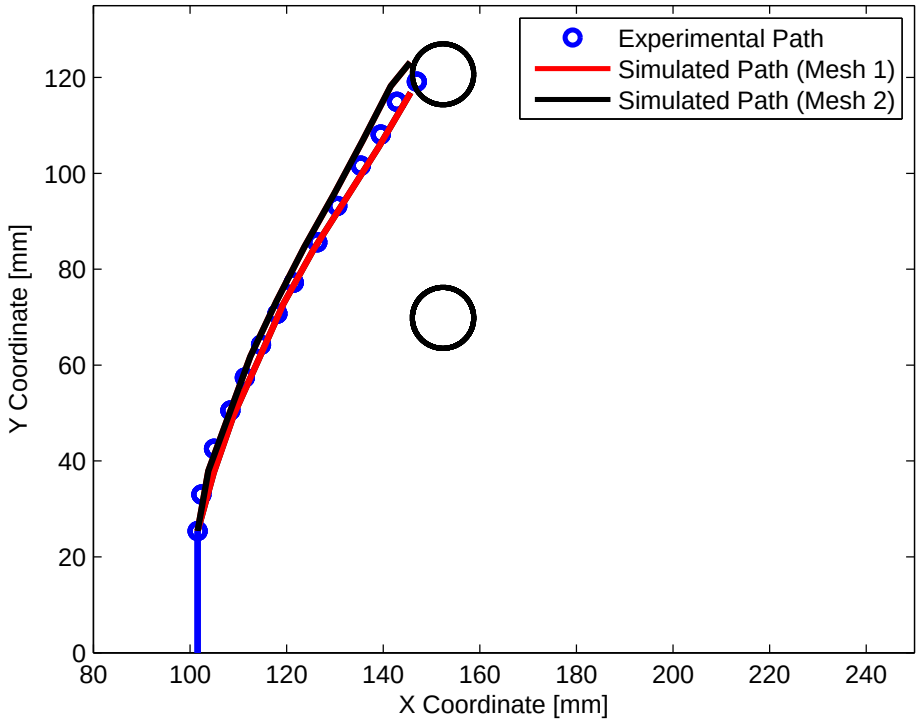

Figure 4.18: Effect of mesh sizes on crack path for specimen 2.

The effect of the amount of crack growth increment is investigated on specimen 6, which has the most curved crack path in experiment. As seen from Figure 4.19, there is no significant difference in simulated crack paths with crack growth increments of 6.35 mm and 12.7 mm. The crack path deviates from the experimental trajectory when a crack growth increment of 25.7 mm is used. Based on the simulations for different crack growth increment and different mesh size, the amount of crack growth increment is taken as 12.7 mm and mesh size used as 1 mm in performing all other simulations.

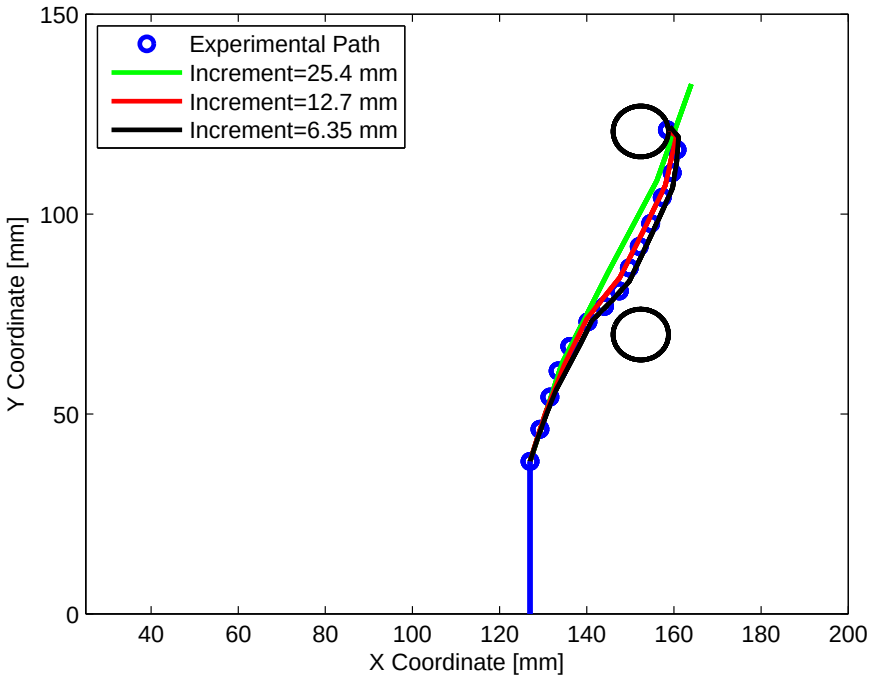

Figure 4.19: Effect of crack growth increment on crack path for specimen 6.

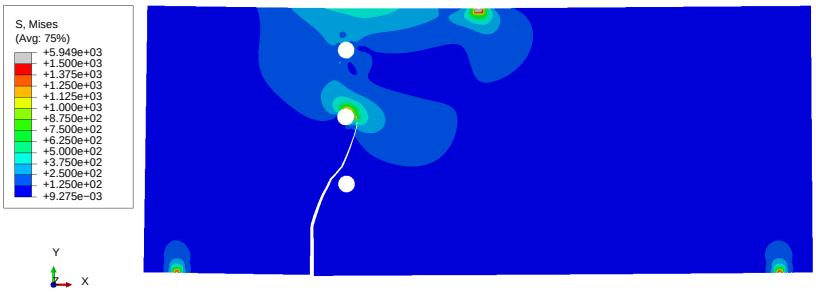

Figure 4.20: Last step of crack path simulation with da=6.35 mm for specimen 6.

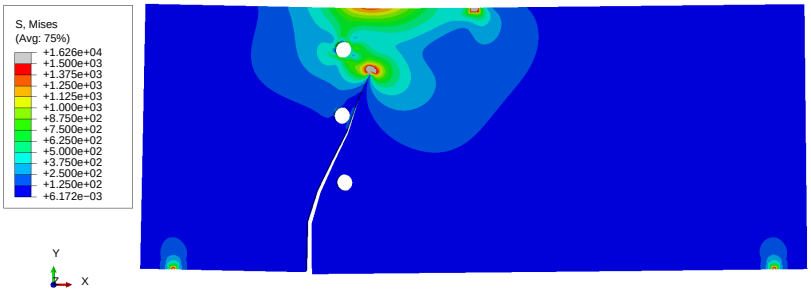

Figure 4.21: Last step of crack path simulation with da=25.7 mm for specimen 6.

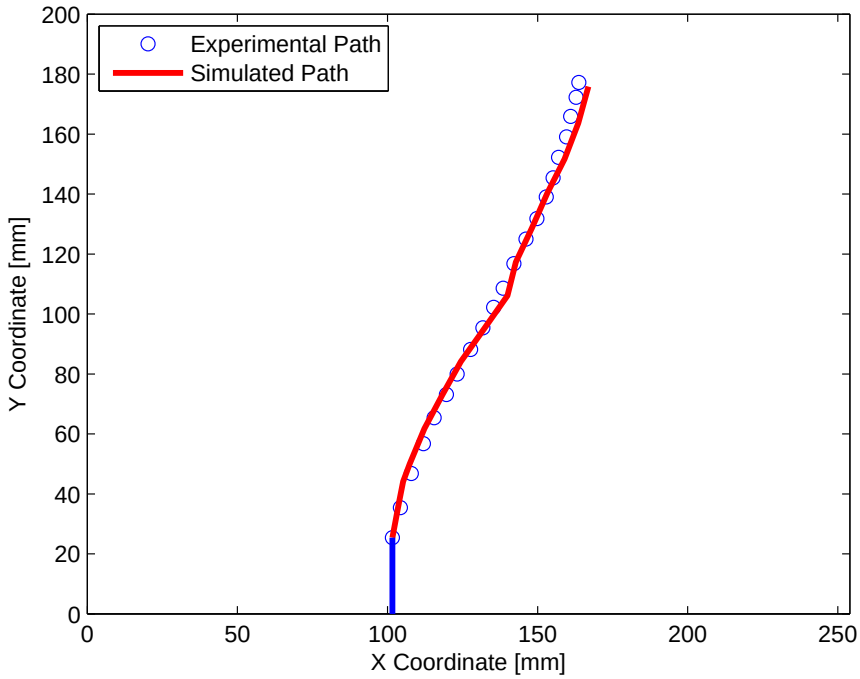

Figure 4.22: Experimental and simulated crack tip coordinates for specimen 1.

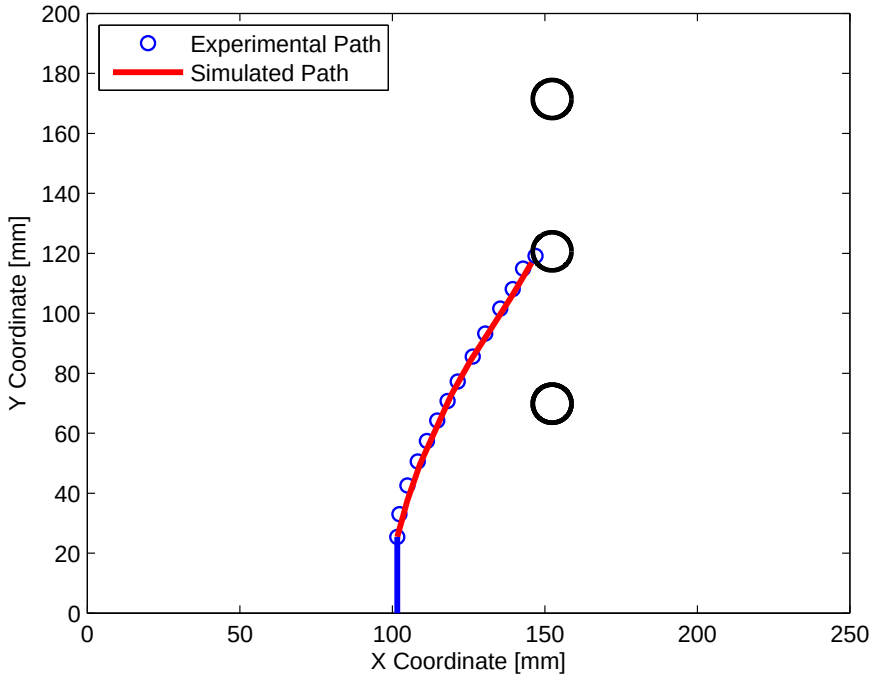

Figure 4.23: Experimental and simulated crack tip coordinates for specimen 2.

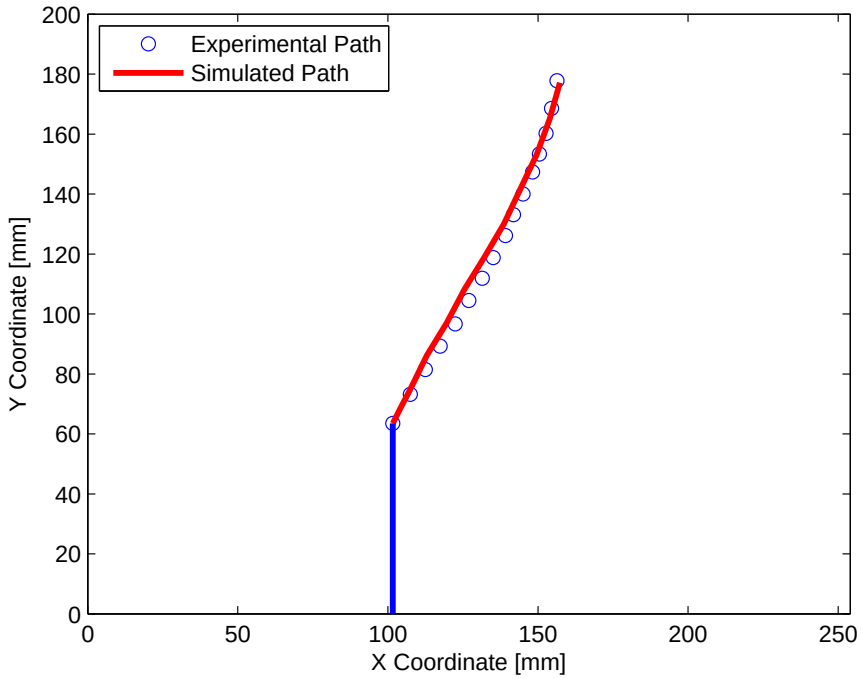

Figure 4.24: Experimental and simulated crack tip coordinates for specimen 3.

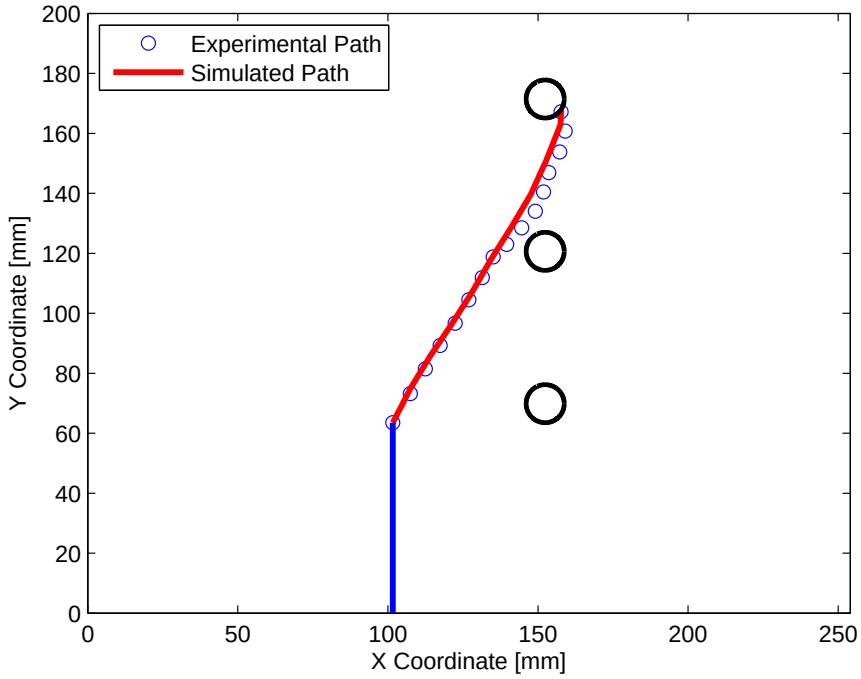

Figure 4.25: Experimental and simulated crack tip coordinates for specimen 4.

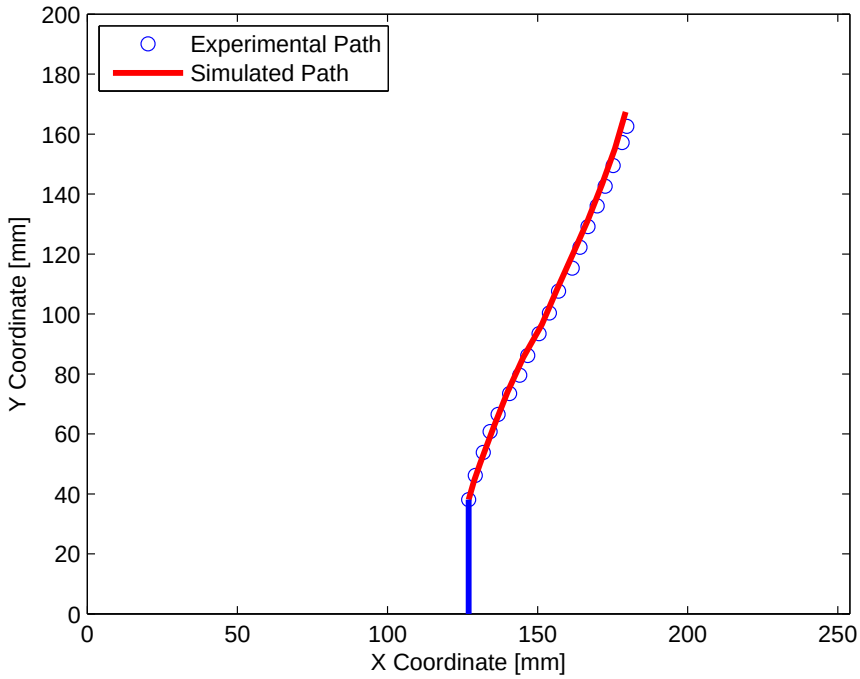

Figure 4.26: Experimental and simulated crack tip coordinates for specimen 5.

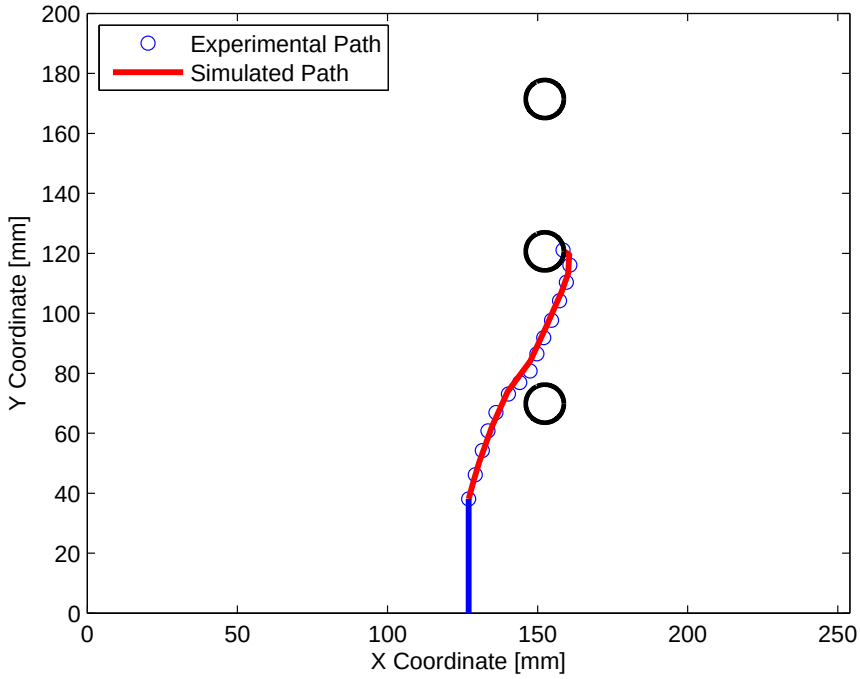

Figure 4.27: Experimental and simulated crack tip coordinates for specimen 6.

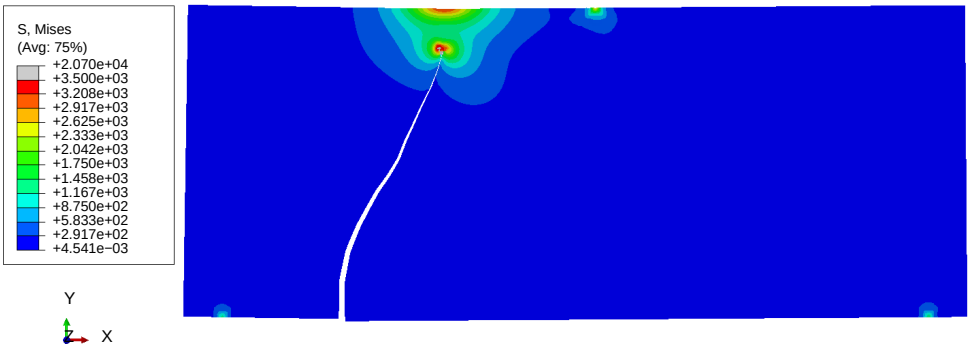

Figure 4.28: Last step of crack growth simulation for specimen 1.

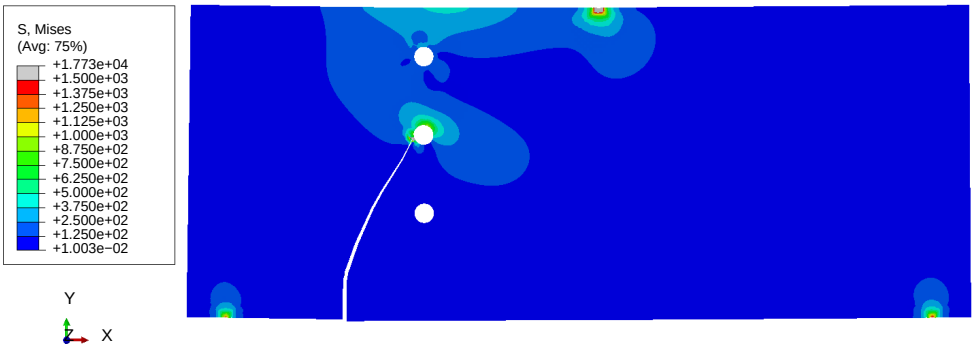

Figure 4.29: Last step of crack growth simulation for specimen 2.

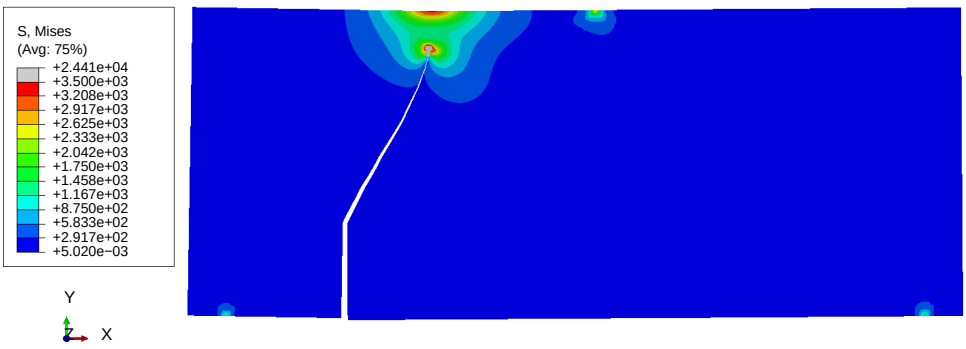

Figure 4.30: Last step of crack growth simulation for specimen 3.

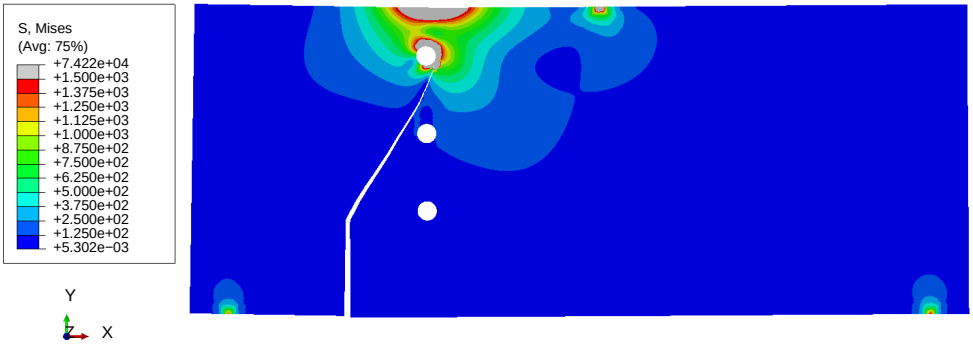

Figure 4.31: Last step of crack growth simulation for specimen 4.

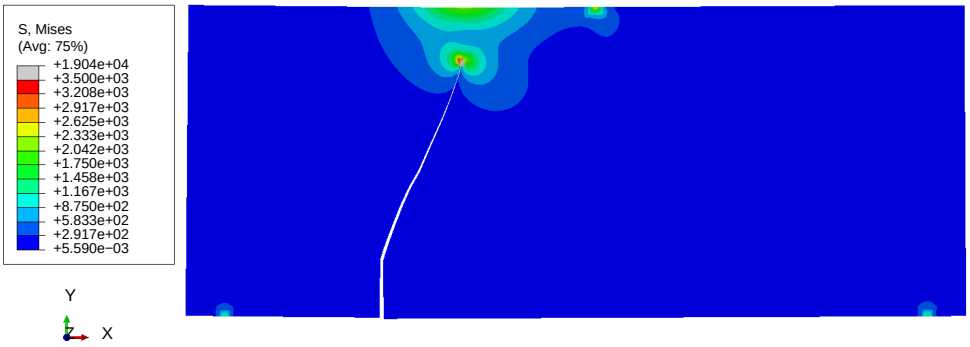

Figure 4.32: Last step of crack growth simulation for specimen 5.

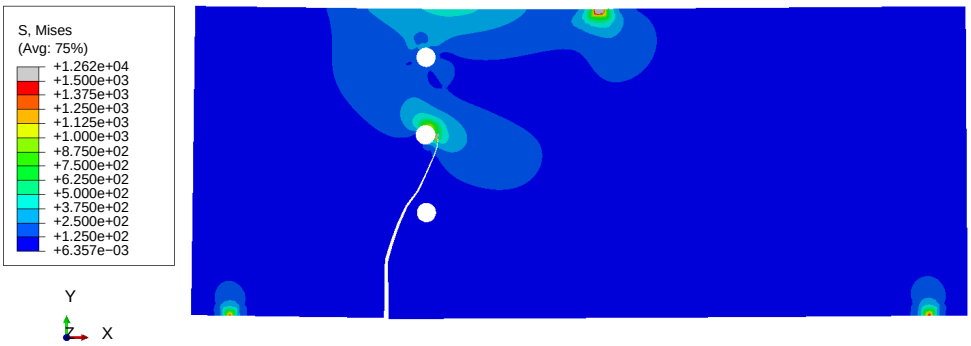

Figure 4.33: Last step of crack growth simulation for specimen 6.

In these series of simulations, holes behave as crack stopper and attract the crack path to propagate towards it as observed in the experimental investigation of the specimens by Ingraffea [52]. In specimen 2, middle hole attracts the crack path and crack stops on this hole. In simulation for specimen 4, since the initial crack length is higher than the specimen 2 the crack path by passes the middle hole and stops in upper hole. In the specimen 6, the first hole attracts the crack path initially due to location of initial crack but the crack by passes it and stop in middle hole again. These results support that the algorithm can be used to locate crack-stopping holes used in designs against damage tolerance. The evaluated results for crack paths have excellent agreements with experimental crack path trajectories as seen from presented results. By these series of simulations crack path trajectory tracking ability of the developed algorithm has been proven to be reliable in mixed mode loading.

4.3 FCG Life and Path Under Mixed Mode Loading I

In this case study, the experimental work conducted by Liu et al. [53] on a Al 7075-T6 hole modified CT specimen is used for demonstrating the ability to predict FCG life in mixed mode loading as well as under CAL and VAL conditions. The hole on the sample was opened to manipulate the crack path towards the hole. The geometrical dimensions of modified CT specimen with and initial crack length of $a = 10.5$ mm are shown in Figure 4.34. The material properties are as follows: elastic modulus $E = 71.7$ GPa, Poisson's ratio $\nu = 0.33$ and yield stress $\sigma_y = 516$ MPa.
Initial FE model of the specimen along with its boundary condition is presented in Figure 4.35. The specimen is constrained in all translational degrees of freedom on its bottom pin location center and the center points are connected to the half bottom region of pin holes by means of coupling connection. It is also constrained in upper pin location in x and z directions, only translation degree of freedom in y direction is left free. A mesh size of 0.4 mm is used in simulation. The constructed FE model of the hole modified CT specimen with the specified initial crack and predetermined crack growth increment of 1 mm is studied through developed simulation algorithm. The automatic propagation process continues until the required final crack size is reached.

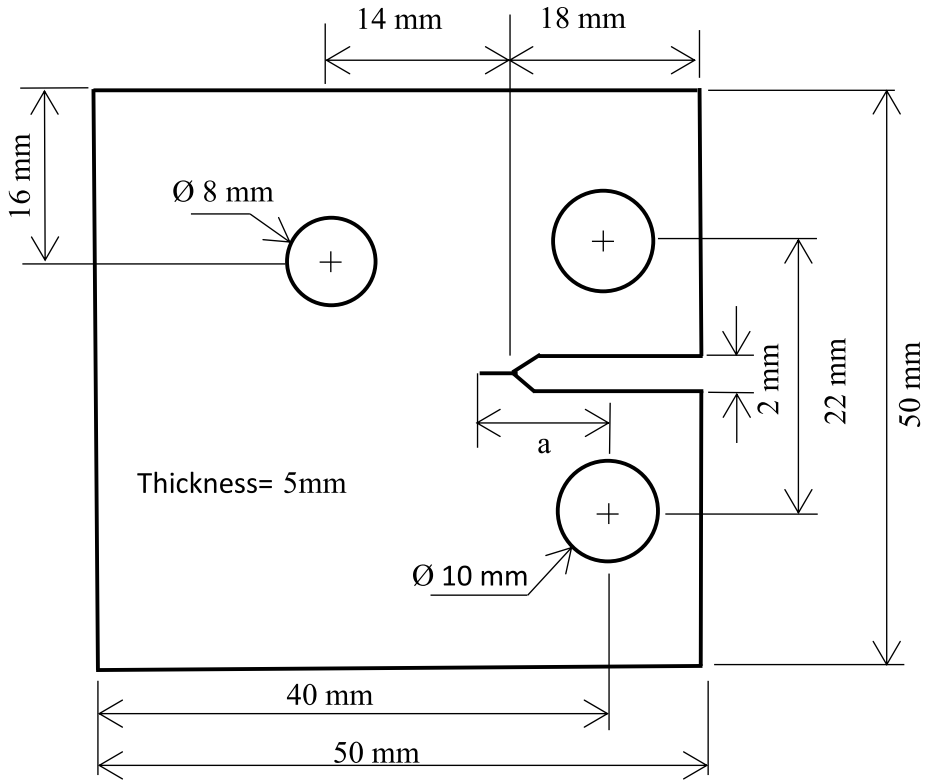

Figure 4.34: Geometrical dimensions for Al 7075-T6 modified CT specimen [53].

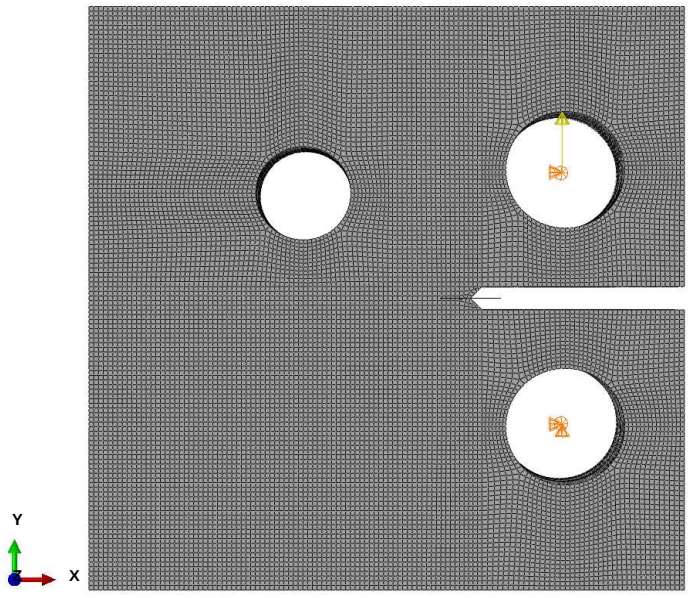

Figure 4.35: FE model for Al 7075-T6 modified CT specimen.

Two types of spectra are used in this case study. The cyclic CAL spectrum has a lower limit of 200 N and a upper limit of 2000 N. For the case of periodic OL (VAL) spectrum, an OL of 3000 N was applied at every 50 cycles of CAL as represented schematically in Figure 4.36.

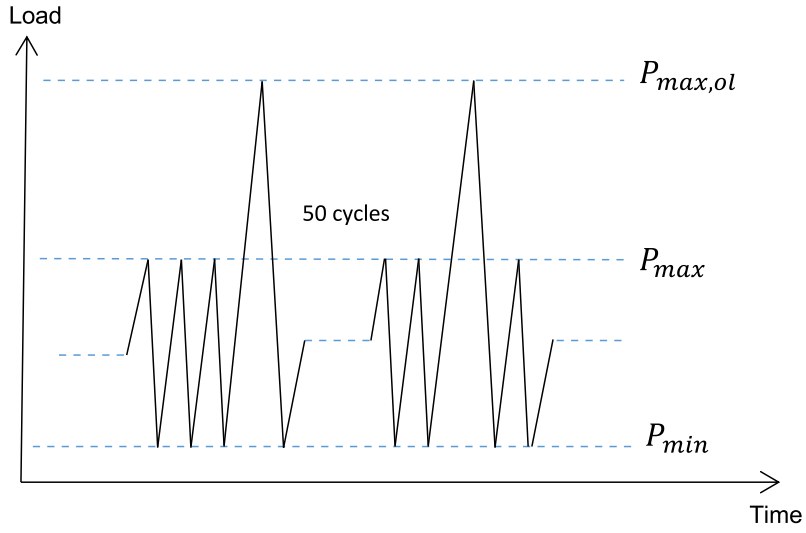

Figure 4.36: Load spectrum for Al 7075-T6 modified CT specimen [53].

Nasgro equation (see 2.11) material parameter C and n calibrated according to CAL test result. Other parameters are used as proposed by Nasgro material database and study conducted by Liu et al. [53]. Nasgro equation parameters used in simulations are presented in Table 4.4.

Table 4.4: Nasgro equation constants for Al 7075-T6 CT specimen [2] [53].

ΔK_{th}	ΔK_{ic}	C	n	p	q	S_{max}/σ_0	α
80 MPa$\sqrt{\text{mm}}$	730 MPa$\sqrt{\text{mm}}$	1.2x10^{-11}	3.0	0.5	1	0.3	2.0

The comparison of simulated and the experimental crack path is presented in Figure 4.37. The hole on CT specimen was specially located to manipulate the crack path towards itself. The last step of crack growth simulations for both constant amplitude and periodic OL case is presented in Figure 4.38. The crack growth paths under constant amplitude and periodic OL are almost identical to each other, which is also demonstrated by our simulations. Since the OL has no effect on crack path a single figure is presented.

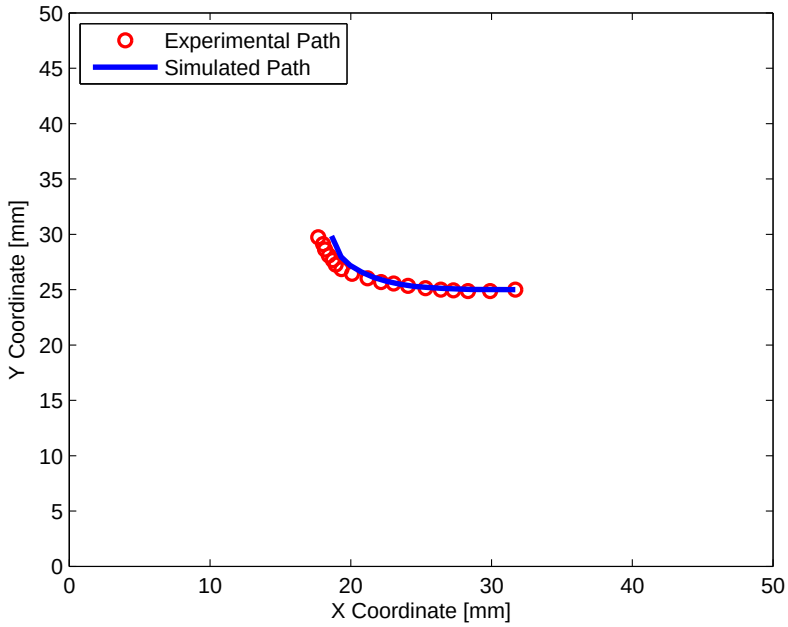

Figure 4.37: Crack tip coordinates for Al 7075-T6 modified CT specimen.

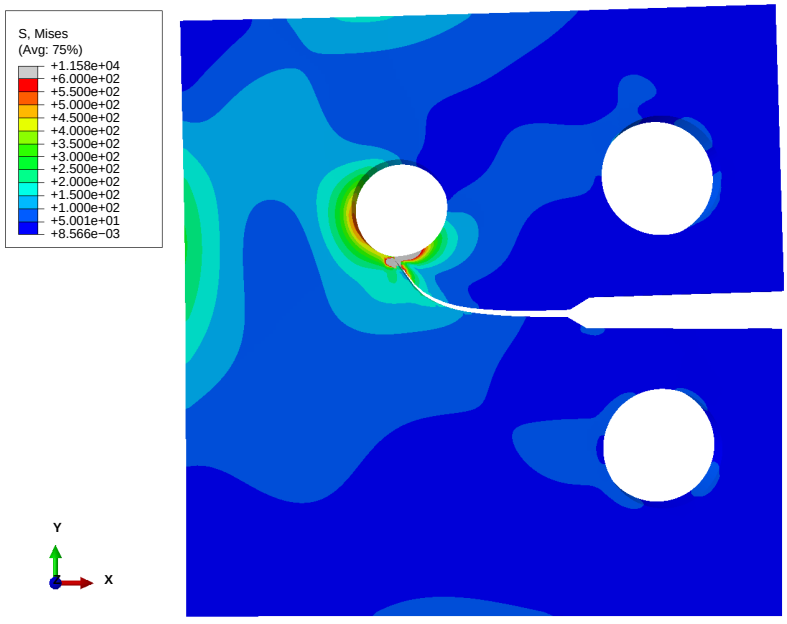

Figure 4.38: Crack growth path for Al 7075-T6 modified CT specimen.

The basic parameter for life evaluation is the SIF. Analytical SIF calculation for standard CT specimen can be found in various handbooks. The analytical SIF solution for standard CT specimen is expressed as follows in [41].

$$K_I = \frac{P f\left(\frac{a}{w}\right)}{B\sqrt{w}} \tag{4.3}$$

where $f\left(\frac{a}{w}\right)$ is the correction factor which depends on crack length to specimen width ratio and represented as follow

$$f\left(\frac{a}{w}\right) = \frac{2+\frac{a}{w}}{\left(1-\frac{a}{w}\right)^{\frac{3}{2}}}\left[0.886 + 4.64\left(\frac{a}{w}\right) - 13.32\left(\frac{a}{w}\right)^2 + 14.72\left(\frac{a}{w}\right)^3 - 5.6\left(\frac{a}{w}\right)^4\right]. \tag{4.4}$$

This handbook solution for correction factor is proposed for mode I loading. In this modified specimen a curved crack path formed due to existence of the hole. The solution for correction factor which is given by equation 4.4 is not valid any more due to curved crack path. The main advantages of mixed mode crack propagation by numerical methods can be seen at this point. The realistic values for $f\left(\frac{a}{w}\right)$ which differ from analytically obtained handbook solutions for standard CT specimen can be obtained by XFEM.

Mode I SIF's at each simulation step is extracted from XFEM solutions and substituted to the equation 4.3 to get the geometry correction factor $f\left(\frac{a}{w}\right)$. A fourth degree polynomial is fitted to the determined correction factors as given in the equation 4.5.

$$f\left(\frac{a}{w}\right) = -2450.1\left(\frac{a}{w}\right)^4 + 4200\left(\frac{a}{w}\right)^3 - 2567.2\left(\frac{a}{w}\right)^2 + 690.21\left(\frac{a}{w}\right) - 63.509 \tag{4.5}$$

The analytically determined correction factor $f\left(\frac{a}{w}\right)$ for standard CT specimen is compared with the correction factor values determined by XFEM for hole modified CT specimen in Figure 4.39. As the curved crack path formed, the $f\left(\frac{a}{w}\right)$ trend diverges from each other.

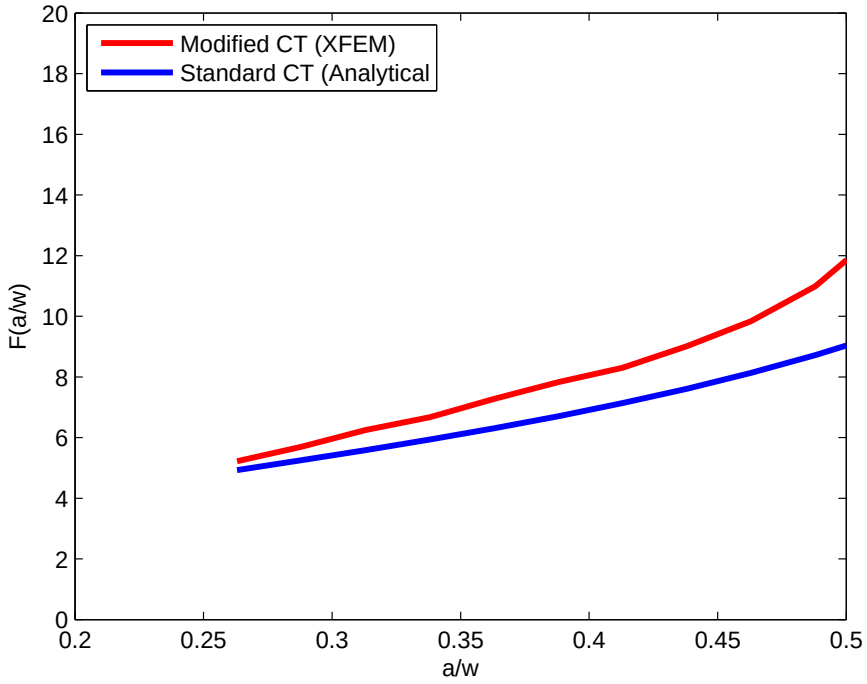

Figure 4.39: $f\left(\frac{a}{w}\right)$ for Al 7075-T6 modified and standard CT specimen.

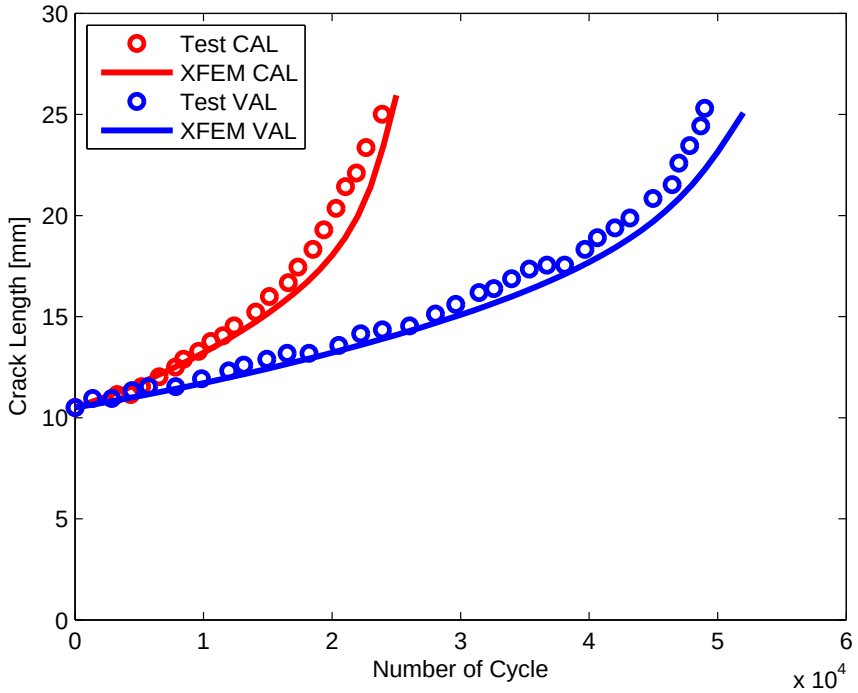

Figure 4.40: FCG life for Al 7075-T6 modified CT specimen for CAL and VAL.

The FCG life is computed through the mixed mode equivalent SIF sugessted by Tanaka [23] (see 2.4) along with Nasgro FCG equation (see 2.11) and Generalized Willenborg retardation model (see 2.24-2.27). Mode I and mode II SIF's are used as follows: $K_I(a)$ along crack length is calculated by using the polynomial fit of the $f\left(\frac{a}{w}\right)$ determined by XFEM solutions, $K_{II}(a)$ expression is also determined from K_{II} values at each propagation step along crack path by fitting a polynomial function in terms of crack length.

Comparison between simulated and experimentally obtained crack length vs. number of loading cycles up to failure for CAL and periodic OL (VAL) spectra are presented in Figure 4.40. As it can be seen from FCG life curve presented for CAL and periodic OL (VAL) spectra, the simulated FCG life by using Generalized Willenborg retardation model have in good agreements with experimental results presented in [53]. The OL delays the FCG life in our simulations by a significant amount around 25.000 cycle as in the case of experimental observation. By this simulation the capability of the developed algorithm in FCG life evaluation under mixed mode loading conditions is proved to be reliable.

4.4 FCG Life and Path Under Mixed Mode Loading II

In the last case study, the developed algorithm is verified again for mixed mode crack propagation in a SAE 1020 hole modified CT specimen with different materials and more complex nature of VAL condition from the previous one to show the versatility of the algorithm in mixed mode VAL conditions. The FCG experimental results which have been performed by Miranda et al. [54] on a SAE 1020 hole modified CT specimen is used for the purpose of validation. The material is cold-rolled SAE 1020 steel plate with yield strength $\sigma_y = 285$ MPa, Young modulus $E = 205$ GPa and Poisson's ratio of $\nu = 0.3$. The geometrical dimensions for modified CT specimen with a initial crack length of $a = 8.3$ mm are shown in Figure 4.41.

Initial FE model of the specimen along with its boundary condition is presented in Figure 4.42. The specimen is constrained in all translational degrees of freedom on its bottom pin location center and the center points are connected to the bottom half

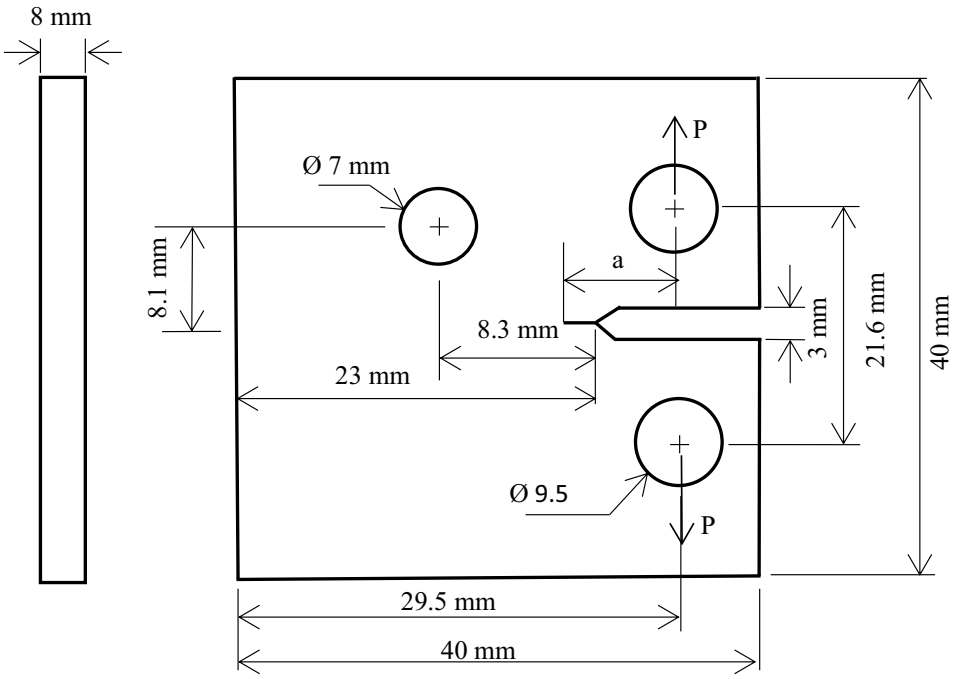

Figure 4.41: Geometrical dimensions of SAE 1020 modified CT specimen [54].

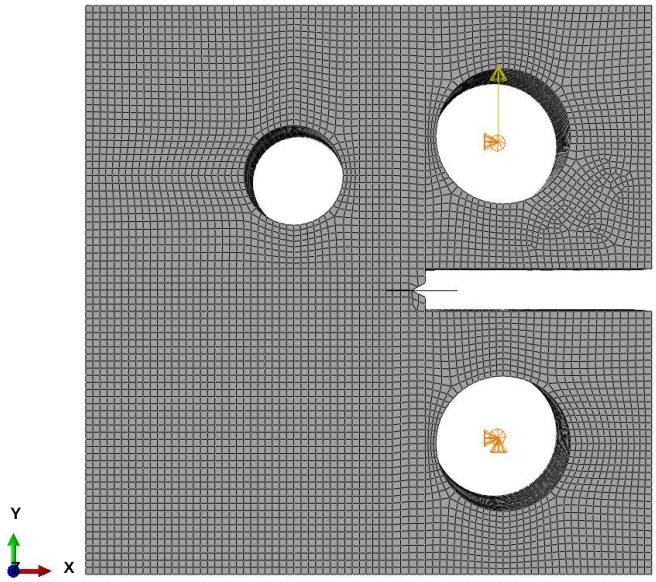

Figure 4.42: FE model for SAE 1020 modified CT specimen.

region of pin holes by means of coupling connection. It is also constrained in upper pin location in x and z directions and only translation degree of freedom in y direction is left free. The constructed FE model of the hole modified CT specimen with the specified initial crack and predefined crack growth increment of 1 mm is simulated. A mesh size of 0.4×0.4 mm is used in simulation. The automatic propagation process continued until the required final crack size was reached. The loading history used in simulation is presented in Figure 4.43.

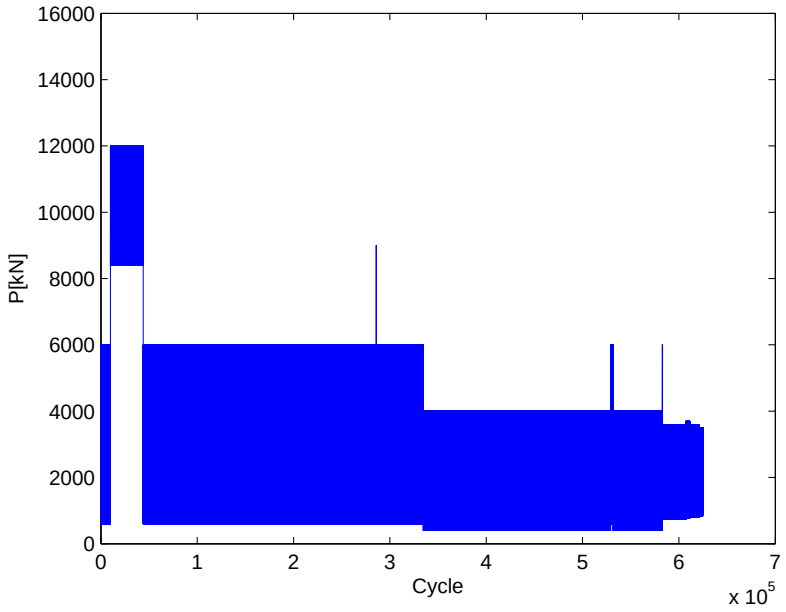

Figure 4.43: Load spectrum for SAE 1020 modified CT specimen [54].

Nasgro equation parameters C and n are calibrated according to experimental results. Other parameters are used as proposed by Nasgro material database [2] and study conducted by Miranda et al. [54]. The parameters of Nasgro equation used in simulation are presented in Table 4.5.

Table 4.5: Nasgro equation constants for SAE 1020 CT specimen [2] [54].

ΔK_{th}	ΔK_c	C	n	p	q	S_{max}/σ_0	α
11.5 MPa$\sqrt{\text{m}}$	285 MPa$\sqrt{\text{m}}$	1.515x10^{-15}	3.7	0.5	0.5	0.5	2.5

In experiment conducted by Miranda et al. [54], the hole on CT specimen was specially located to manipulate the crack path. In our simulation, the crack path was

initially attracted by the hole but it by passes the hole and continues to propagate in a straight direction as in the case of experiment. Comparison of simulated and experimental crack path is presented in Figure 4.44. The last step of crack path from XFEM simulation is also given in Figure 4.45.

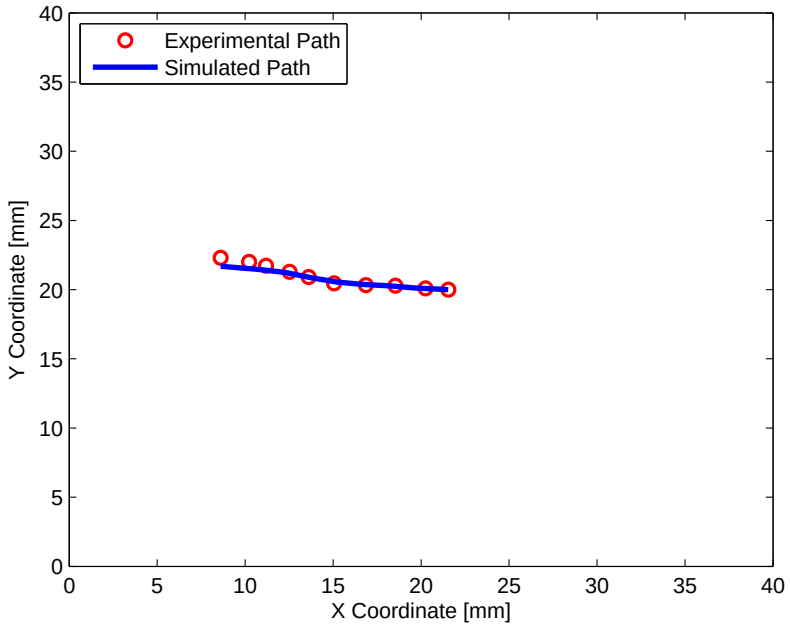

Figure 4.44: Crack tip coordinates for SAE 1020 modified CT specimen.

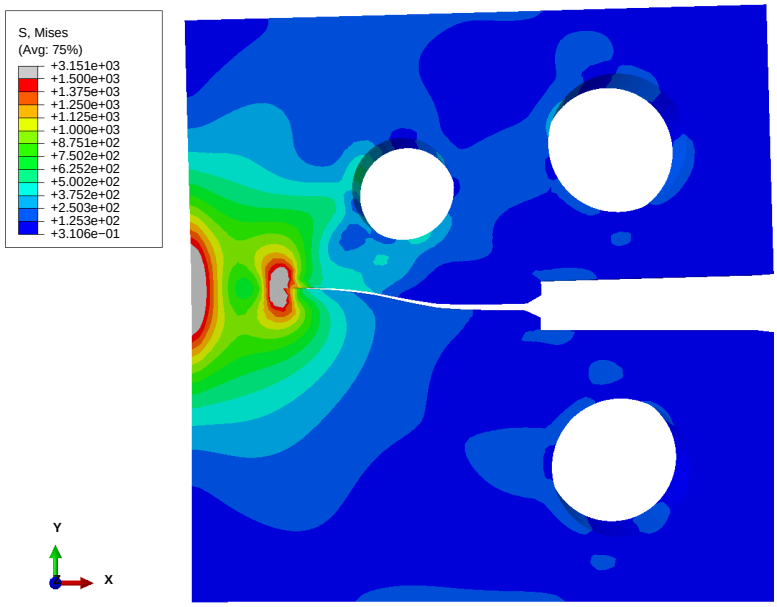

Figure 4.45: Crack growth path for SAE 1020 modified CT specimen.

Mode I SIF's at each simulation step is extracted from XFEM solutions and substituted to the equation 4.3 to get the geometry correction factor $f\left(\frac{a}{w}\right)$. A fourth degree polynomial is fitted to the determined correction factors as given in the equation 4.6.

$$f\left(\frac{a}{w}\right) = 1070.8\left(\frac{a}{w}\right)^4 - 1931.8\left(\frac{a}{w}\right)^3 + 1318.9\left(\frac{a}{w}\right)^2 - 376.22\left(\frac{a}{w}\right) + 43.263 \tag{4.6}$$

The analytically determined correction factor $f\left(\frac{a}{w}\right)$ from equation 4.4 for standard CT specimen is compared with the values determined by XFEM for hole modified CT specimen in Figure 4.46.

The FCG life is computed through the mixed mode equivalent SIF sugessted by Tanaka [23] (see 2.4) along with Nasgro FCG equation (see 2.11) and Modified Wheeler retardation model (see 2.23). Mode I and mode II SIF's are used as follows: $K_I(a)$ along crack length is calculated by using the polynomial fit of the $f\left(\frac{a}{w}\right)$, $K_{II}(a)$ expression is also determined from $K_{II}(a)$ values at each propagation step by fitting a polynomial function in terms of crack length.

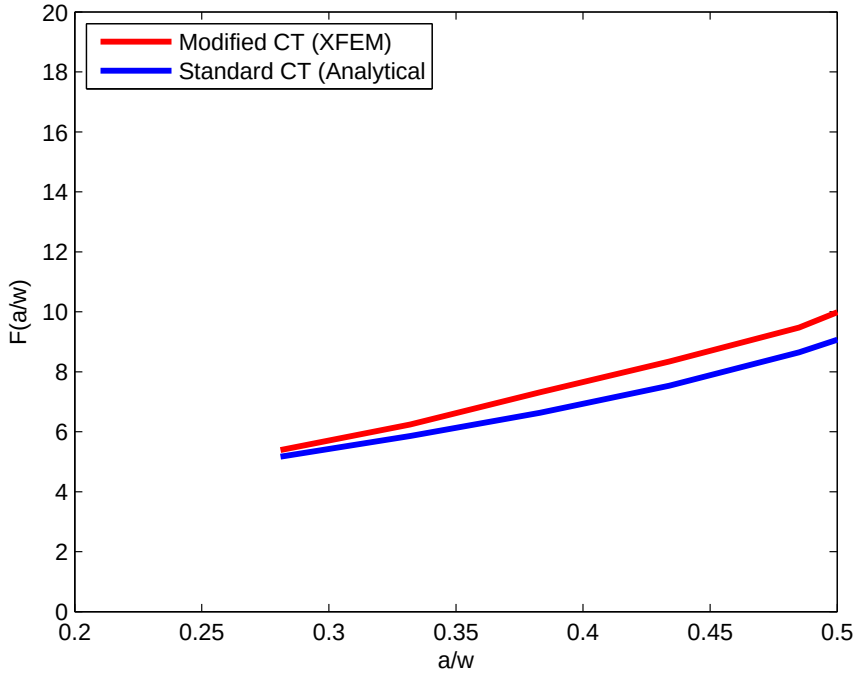

Figure 4.46: $f(a/w)$ for SAE 1020 modified and standard CT specimen.

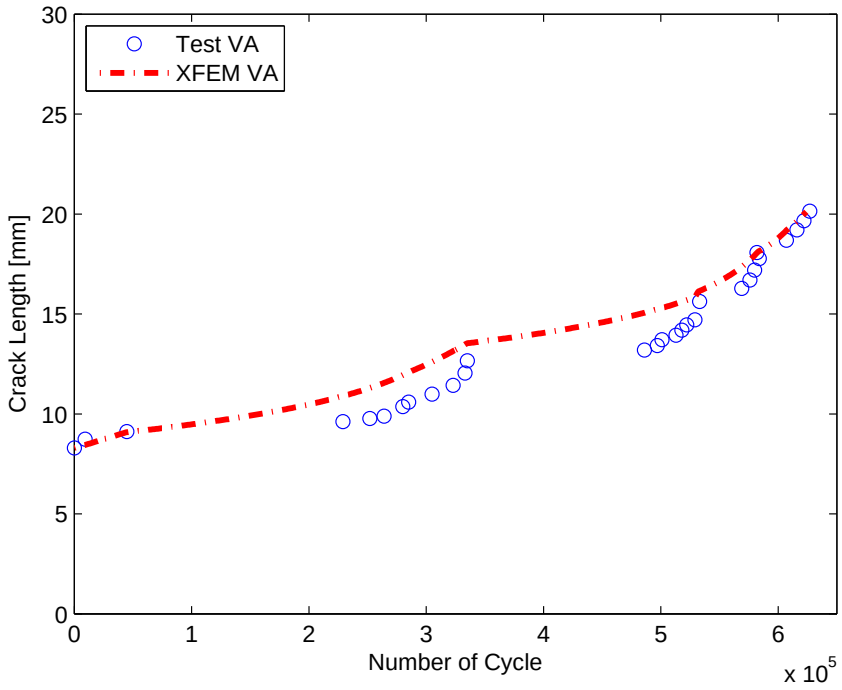

Figure 4.47: FCG life for SAE 1020 modified CT specimen.

Modified Wheeler Retardation parameter for straight crack propagation on the standard CT specimen under the same loading nature was determined by Miranda et al. [54] as 0.51. The resulting finding of Miranda et al. showed that, load interaction models calibrated using straight cracks can be used safely to predict retardation behaviour of non planar cracks under the similar nature of VAL conditions. Reasonable results are obtained for crack path and fatigue life under the defined complex loading spectrum by using the Modified Wheeler retardation parameter based on Miranda's work. Comparison between simulated and experimental crack length vs. number of loading cycles up to failure is presented in Figure 4.47. The FCG is predicted as the same trend in test with some minor discrepancy related with material and test parameters.

CHAPTER 5

CONCLUSION

In this thesis, an automated XFEM-based FCG tool which allows mesh independent crack insertion and growth is presented for the estimation of crack propagation path and FCG life. XFEM was used to calculate the SIF's and crack path at each propagation step without re-meshing burden. Although the main purpose of the study is to determine the crack path, it can effectively predict the FCG life with the realistic material parameters under either CAL or VAL conditions by accounting the load history effects.

Stationary crack modelling technique was used and crack was propagated by a Fortran script. By this way, full enrichment capability of Abaqus on stationary cracks is used which is not applied to propagating cracks in Abaqus. Moreover, the convergence problems encountered in the solution of propagating cracks with XFEM in Abaqus are eliminated. Stepwise crack propagation process gives more control and the analysis possibility to the user since it is not needed to propagate crack at every load cycle. There is an improvement in the computational efficiency compared to Abaqus self-crack propagation simulation which has heavy cost in computational means.

As an important contribution, unlike standard implementation of XFEM in Abaqus for propagating cracks, developed algorithm uses LEFM based approach and it can be used in damage tolerance assessments where there is a necessity for LEFM based approaches.

In this algorithm, the crack propagation path and fatigue life was calculated by using a cycle-by-cycle integration method considering overload retardation effects. Aforementioned retardation effect has significant improvements on the FCG life and would result in conservative consequences if not included in the calculations as demonstrated by presented case studies. This conservatism has been prevented by using appropriate retardation models according to nature of the loads.

Developed numerical algorithm is validated successfully by conducting general curvilinear FCG simulations under both CAL and VAL spectra. Four different specimens are examined under different load spectra having different configurations in terms of crack growth path and fatigue life.

In the first case study, an internal cracked tension specimen is analysed through a total of seven different loading spectra with a CAL spectrum. In this case study the crack path is planar due to applied uni-axial loading as expected and doesn't change its direction during simulations. The main interest in this study was to demonstrate FCG life evaluation capability. The obtained FCG life by using modified generalized Willenborg model is compared with Nasgro software and available test results. There is a quite a good agreement in this comparative study in terms of FCG lives.

In the second case study, a three point bending PMMA specimen is considered. The main goal in this study is to verify the code in terms of crack path under mixed mode loading. A total of six configurations of specimen are simulated with and without hole configurations. The obtained crack path has excellent agreement with available test results. By this series of simulations crack path evaluation capability has been demonstrated.

In the third case study, a hole modified CT specimen is analysed under CAL and VAL mixed mode conditions. The generalized modified Willenborg model is incorporated into the algorithm for this case study. The FCG life results with calibrated material parameters based on Nasgro material database has good agreements with experimental results.

As the last case study, a hole modified CT specimen with different dimensions, materials and more complex loading nature from the previous one is considered. In this case , modified Wheeler model is adopted to the code to cover the retardation effect. The FCG life with calibrated material parameters based on Nasgro material database has good agreements with experimental result.

Validation with experimental results shows that the presented numerical methodology could effectively simulate the crack propagation paths and fatigue lives under either mode I or mixed mode loading condition. The developed code may have application areas as follows. Users can identify fatigue critical regions where the cracks are likely to occur and crack propagation trajectory can be found through this numerical algorithm. Crack stopping measures can be taken on the predicted crack path trajectories such as crack stopper holes or any other design solutions. The user can also use this algorithm in life estimations of standard and modified test samples and industrial components.

The results of this study show that based on the advantageous fracture modelling capabilities of XFEM, cost effective and practical computational algorithm in the application of the FCG path and life prediction under mixed mode practical service loading conditions is possible by algorithms which use externally defined analytical methods. The obtained accuracy of XFEM in predicting FCG under VAL in an automated scheme gives the users the confidence to apply the methodology to industrial components under complex service loading conditions. The outlook for future works can be summarized as follows,

- Different crack path prediction models can be employed for crack path evaluations.
- Different crack growth rate equations and retardation models can be implemented and used for comparison purpose in analytical fatigue life estimations.
- Experiments on other materials and geometries can be conducted and compared by the results obtained from the developed XFEM based algorithm.
- Conventional FEM based analysis or other type of methods can be developed

and compared with the XFEM based methodology in terms of computational performance practicability and reliability.

- Through the developed FCG algorithm real industrial components under realistic fatigue spectrum loadings could be analysed.

REFERENCES

[1] J. A. Harter. Afgrow users guide and technical manual. *AFRL-VA-WP-TR-2006, AFGROW, version 4.0011.14*, 2006.

[2] Nasgro. Fracture mechanics and fatigue crack growth analysis software (version 4.02), reference manual. *NASA Johnson Space Center and Southwest Research Institute*, 2002.

[3] Kiran Solanki, S.R Daniewicz, and J.C Newman Jr. Finite element modeling of plasticity-induced crack closure with emphasis on geometry and mesh refinement effects. *Eng. Fract. Mech.*, 70(12):1475 – 1489, 2003.

[4] Giovanni Formica and Franco Milicchio. Crack growth propagation using standard {FEM}. *Engineering Fracture Mechanics*, 165:1 – 18, 2016.

[5] I. Varfolomeev, M. Burdack, S. Moroz, D. Siegele, and K. Kadau. Fatigue crack growth rates and paths in two planar specimens under mixed mode loading. *International Journal of Fatigue*, 58:12 – 19, 2014.

[6] T. Belytschko and T. Black. Elastic crack growth in finite elements with minimal remeshing. *International Journal for Numerical Methods in Engineering*, 45:601–620, June 1999.

[7] J.M. Melenk and I. Babuska. The partition of unity finite element method: Basic theory and applications. *Comput. Methods in Appl. Mech. Eng.*, 139(1–4):289 – 314, 1996.

[8] Jianxu Shi, David Chopp, Jim Lua, N. Sukumar, and Ted Belytschko. Abaqus implementation of extended finite element method using a level set representation for three-dimensional fatigue crack growth and life predictions. *Engineering Fracture Mechanics*, 77(14):2840 – 2863, 2010.

[9] N. Sukumar and J.-H. Prévost. Modeling quasi-static crack growth with the extended finite element method part i: Computer implementation. *International Journal of Solids and Structures*, 40(26):7513 – 7537, 2003.

[10] Stéphane Bordas and Brian Moran. Enriched finite elements and level sets for damage tolerance assessment of complex structures. *Engineering Fracture Mechanics*, 73(9):1176 – 1201, 2006.

[11] E. Giner, N. Sukumar, J.E. Tarancón, and F.J. Fuenmayor. An abaqus implementation of the extended finite element method. *Engineering Fracture Mechanics*, 76(3):347 – 368, 2009.

[12] F. Amiri, C. Anitescu, M. Arroyo, S. P. A. Bordas, and T. Rabczuk. Xlme interpolants, a seamless bridge between xfem and enriched meshless methods. *Comput. Mech.*, 53(1):45–57, 2013.

[13] M.C. Baietto, E. Pierres, A. Gravouil, B. Berthel, S. Fouvry, and B. Trolle. Fretting fatigue crack growth simulation based on a combined experimental and {XFEM} strategy. *Int J. Fract.*, 47:31 – 43, 2013.

[14] Dassault Systemes AD. *Abaqus User Guide*. 2014.

[15] R Plank and G Kuhn. Fatigue crack propagation under non-proportional mixed mode loading. *Engineering Fracture Mechanics*, 62(2–3):203 – 229, 1999.

[16] Slobodanka Boljanović and Stevan Maksimović. Analysis of the crack growth propagation process under mixed-mode loading. *Engineering Fracture Mechanics*, 78(8):1565 – 1576, 2011. Multiaxial FractureMultiaxial Fracture.

[17] Miaolin Feng, Fei Ding, and Yanyao Jiang. A study of loading path influence on fatigue crack growth under combined loading. *International Journal of Fatigue*, 28(1):19 – 27, 2006.

[18] B. Cotterell and J.R. Rice. Slightly curved or kinked cracks. *International Journal of Fracture*, 16(2):155–169, 1980.

[19] O. E. Wheeler. Spectrum loading and crack growth. *J. Basic Eng.*, 94:181–186, 1972.

[20] R. M. Willenborg, J. P. Engle and H. A. Wood. A crack growth retardation model using an effective stress concept. *AFFDL-TM-71-1-FBR*, 1971.

[21] Haydar Dirik and Tuncay Yalçinkaya. Fatigue crack growth under variable amplitude loading through {XFEM}. *Procedia Structural Integrity*, 2:3073 – 3080, 2016. 21st European Conference on Fracture, ECF21, 20-24 June 2016, Catania, Italy.

[22] Haydar Dirik and Tuncay Yalçinkaya. Crack growth analysis under variable amplitude loading by {XFEM}. VI.National Aviation and Space Conference , 28-30 September 2016, Kocaeli, Turkey.

[23] Keisuke Tanaka. Fatigue crack propagation from a crack inclined to the cyclic tensile axis. *Engineering Fracture Mechanics*, 6(3):493–507, oct 1974.

[24] H.A. Richard. Fracture predictions for cracks exposed to superimposed normal and shear stresses. 1985.

[25] Yan Xiangqiao, Du Shanyi, and Zhang Zehua. Mixed-mode fatigue crack growth prediction in biaxially stretched sheets. *Engineering Fracture Mechanics*, 43(3):471 – 475, 1992.

[26] Erdogan, F.; Sih, and G. C. On the crack extension in plates under plane loading and transverse shear. *Transactions of the ASME. Series D, Journal of Basic Engineering*, 85(4), 1963.

[27] D.F. Socie, C.T. Hua, and D.W. Worthem. Mixed mode small crack growth. *Fatigue and Fracture of Engineering Materials and Structures*, 10(1):1–16, 1987.

[28] T. Hoshide and D.F. Socie. Mechanics of mixed mode small fatigue crack growth. *Engineering Fracture Mechanics*, 26(6):841–850, 1987.

[29] L.M. Keer W.R. Chen. Fatigue crack growth in mixed mode loading. *J Engng Mater Technol ASME Trans*, 85(113):223–227, 1991.

[30] P Paris and F Erdogan. A Critical Analysis of Crack Propagation Laws. *Journal of Basic Engineering*, 85(4):528–533, dec 1963.

[31] K Walker. Effects of environment and complex load history on fatigue life, astm stp 462. In *American Society for Testing and Materials*, pages 1–14, 1970.

[32] R G Forman, V E Kearney, and R M Engle. Numerical Analysis of Crack Propagation in Cyclic-Loaded Structures. *Journal of Basic Engineering*, 89(3):459–463, sep 1967.

[33] A. Hartman and J. Schijve. The effects of environment and load frequency on the crack propagation law for macro fatigue crack growth in aluminium alloys. *Eng. Fract. Mech.*, 1(4):615 – 631, 1970.

[34] S. R. Forman, R. G. Mettu. Behavior of surface and corner cracks subjected to tensile and bending loads in ti-6al-4v alloy. *ASTM STP 1131*, pages 519–546, 1992.

[35] J. C. Newman. A crack closure model for predicting fatigue crack growth under aircraft spectrum loading. *ASTM-STP*, 748:53–84, 1981.

[36] B. Moreno, A. Martin, P. Lopez-Crespo, J. Zapatero, and J. Dominguez. Estimations of fatigue life and variability under random loading in aluminum al-2024t351 using strip yield models from {NASGRO}. *International Journal of Fatigue*, 91, Part 2:414 – 422, 2016.

[37] M. Sander and H.A. Richard. Investigations on fatigue crack growth under variable amplitude loading in wheelset axles. *Engineering Fracture Mechanics*, 78(5):754 – 763, 2011.

[38] Rui Bao and Xiang Zhang. Fatigue crack growth behaviour and life prediction for 2324-t39 and 7050-t7451 aluminium alloys under truncated load spectra. *Int. J. Fatigue*, 32(7):1180 – 1189, 2010.

[39] G. C. Sih. Strain-energy-density factor applied to mixed mode crack problems. *International Journal of Fracture*, 10(3):305–321, 1974.

[40] K. Palaniswamy and W.G. Knauss. {II} - on the problem of crack extension in brittle solids under general loading. In S. NEMAT-NASSER, editor, *Mechanics Today*, pages 87 – 148. Pergamon, 1978.

[41] J. Schijve, Fatigue of Structures and Materials 2nd edition. Kluwer Akademic Publisher, (2001).

[42] S K Maiti and R A Smith. Comparison of the criteria for mixed mode brittle fracture based on the preinstability stress-strain field Part I: Slit and elliptical cracks under uniaxial tensile loading. *International Journal of Fracture*, 23(4):281–295, 1983.

[43] J. Qian and A. Fatemi. Mixed mode fatigue crack growth: A literature survey. *Engineering Fracture Mechanics*, 55(6):969 – 990, 1996.

[44] Marco Antonio Meggiolaro and Jaime Tupiassú Pinho de Castro. An evaluation of elber-type crack retardation models. In *SAE Technical Paper*. SAE International, 03 2001.

[45] M.A. Meggiolaro, A.C.O. Miranda, J.T.P. Castro, and L.F. Martha. Stress intensity factor equations for branched crack growth. *Engineering Fracture Mechanics*, 72(17):2647 – 2671, 2005.

[46] J.P. Gallagher and T.F. Hughes. Influence of yield strength on overload affected fatigue crack growth behaviour in 4340 steel. *AFFDL-TR-74-28*, 1974.

[47] T. R. Brussat. Private communication. 1997.

[48] N. Moës, A. Gravouil, and T. Belytschko. Non-planar 3d crack growth by the extended finite element and level sets—part i: Mechanical model. *International Journal for Numerical Methods in Engineering*, 53(11):2549–2568, 2002.

[49] A. Gravouil, N. Moës, and T. Belytschko. Non-planar 3d crack growth by the extended finite element and level sets—part ii: Level set update. *International Journal for Numerical Methods in Engineering*, 53(11):2569–2586, 2002.

[50] C. Shih, B. Moran, T. Nakamura. Energy release rate along a three-dimensional crack front in a thermally stressed body *International Journal of Fracture*, 30(2):79–102, 1986.

[51] Theodore R. Porter. Method of analysis and prediction for variable amplitude fatigue crack growth. *Eng. Fract. Mech.*, 4(4):717 – 736, 1972.

[52] Anthony. R. Ingraffea. Probabilistic fracture mechanics:a validation of predictive capability. Department of Structural Engineering. Technical report, Cornell University, 1990.

[53] Zizi Lu, Jifeng Xu, Lei Wang, Jianren Zhang, and Yongming Liu. Curvilinear fatigue crack growth simulation and validation under constant amplitude and overload loadings. *Journal of Aerospace Engineering*, 28(1), 1 2015.

[54] Antonio Carlos de Oliveira Miranda, Marco Antonio Meggiolaro, Jaime Tupiassú Pinho de Castro, and Luiz Fernando Martha. Fatigue life prediction of complex 2d components under mixed-mode variable amplitude loading. *International Journal of Fatigue*, 25(9–11):1157 – 1167, 2003. International Conference on Fatigue Damage of Structural Materials {IV}.

[55] M. Naderi and N. Iyyer. Fatigue life prediction of cracked attachment lugs using {XFEM}. *International Journal of Fatigue*, 77:186 – 193, 2015.